A Domain-general Cognitive Core defined in Multimodally Parcellated Human Cortex

Moataz Assem[1*], Matthew F. Glasser[2,3,4], David C. Van Essen[2], John Duncan[1,5]

[1] MRC Cognition and Brain Sciences Unit, University of Cambridge, Cambridge, UK

[2] Department of Neuroscience, Washington University in St. Louis, Saint Louis, MO, USA

3 Department of Radiology, Washington University in St. Louis, Saint Louis, MO, USA

[4] St. Luke's Hospital, Saint Louis, MO, USA

[5] Department of Experimental Psychology, University of Oxford, Oxford, UK

*corresponding author: moataz.assem@mrc-cbu.cam.ac.uk

Abstract

Countless brain imaging studies document "multiple-demand" (MD) regions co-activated by a broad domain of tasks, but with little consensus over exact anatomy and functional properties. To overcome these limitations, we use data from 449 subjects from the Human Connectome Project, with cortex of each individual parcellated using neurobiologically grounded multi-modal MRI features. In contrast to unfocused swathes of activation, the conjunction of three cognitive contrasts reveals a core of 10 widely distributed MD regions per hemisphere that are most strongly activated and functionally interconnected, surrounded by a penumbra of 17 further regions. Subcortically, MD activity is seen especially in the caudate and cerebellum. Comparison with canonical resting state networks shows MD regions concentrated in the fronto-parietal network but extending into three other networks. MD activations show modest relative task preferences accompanying strong co-recruitment. With precise anatomical delineation, we offer a basis for cumulative study of MD functions and their role in the assembly of flexible cognitive structures.

Keywords

Multiple-demand; multi-modal; cortical parcellation; executive functions; cognitive control; working memory; reasoning; math; fronto-parietal; resting state; domain-general.

Introduction

Thought and behavior can be conceptualized as complex cognitive structures within which simpler steps are combined to achieve an overall goal (Luria, 1966; Miller et al., 1968; Newell, 1990). Each step or cognitive episode involves a rich combination of relevant external and internal inputs, computations, and outputs, assembled into the appropriate relations as dictated by current needs. A system capable of such behavior must be equipped with a flexible control structure that can appropriately select, modify and assemble each cognitive step on demand.

In line with a system's role in organizing complex cognition, selective damage to specific regions in the frontal and parietal cortex is associated with disorganized behavior (Luria, 1966; Milner, 1963; Norman and Shallice, 1986), including significant losses in fluid intelligence (Duncan et al., 1995; Glascher et al., 2010; Roca et al., 2010; Warren et al., 2014; Woolgar et al., 2018, 2010). Numerous functional neuroimaging studies converge on a similar set of frontal and parietal regions that are co-activated when performing a diverse range of cognitively demanding tasks, including selective attention, working memory, problem solving, response inhibition and much more (Cole and Schneider, 2007; Duncan and Owen, 2000; Fedorenko et al., 2013; Hugdahl et al., 2015). We refer to this network of regions as the multiple-demand (MD) system, reflecting their co-recruitment by multiple task demands (Duncan, 2013, 2010). MD activity is commonly seen in lateral and dorsomedial prefrontal cortex, in the anterior insula, and within and surrounding the intraparietal sulcus, with an accompanying activation often reported near the occipito-temporal border. Many resting-state fMRI (rfMRI) studies report a similar (but not identical as we will demonstrate) "fronto-parietal" network whose components show strongly correlated time series (Ji et al., 2019; Laumann et al., 2015; Power et al., 2011; Yeo et al., 2011), parts of which are proposed to act as communication hubs owing to their connectivity patterns with other cortical networks (Gordon et al., 2018; Power et al., 2013). Cortical MD regions are also associated with subcortical regions that are co-activated across multiple tasks and are strongly functionally connected with the MD cortex. Though much less studied, these are putatively distributed in restricted sub regions of the basal ganglia, thalamus and cerebellum (Buckner et al., 2011; Choi et al., 2016; Halassa and Kastner, 2017).

In non-human primates, fMRI studies have identified a putative cortical MD network organized in anatomically similar and likely evolutionarily homologous regions (Ford et al., 2009; Mitchell et al., 2016; Premereur et al., 2018). Single-neuron studies in these regions reveal highly dynamic and adaptive neural activity patterns that encode many kinds of task-relevant information such as stimulus features, goals, actions, rules and rewards (Duncan, 2001; Miller and Cohen, 2001; Stokes et al., 2013). Further, these neurons are characterized by their mixed selectivity, i.e., activity driven by complex conjunctions of relevant stimuli, processes and task events (Fusi et al., 2016; Naya et al., 2017; Rigotti et al., 2013; Sigala et al., 2008). With access to many kinds of information, adaptive neural activity, and conjunctive coding of task-relevant

information, the MD system is well positioned to assemble the rich, integrated control structures of complex behavior (Duncan, 2013). Like a skeleton, the MD system is hypothesized to support the assembly of each task episode by integrating processing in multiple brain regions to access and bind the required information and cognitive operations (Dehaene et al., 1998; Desimone and Duncan, 1995; Miller and Cohen, 2001; Norman and Shallice, 1986).

While MD activity has been reported since the early days of human brain imaging (Duncan and Owen, 2000), there remains little consensus over core questions including the precise anatomy of MD regions, their differentiation from nearby regions with quite different functional properties, their functional specializations and their connectivity. In large part, we suggest, the lack of cumulative progress reflects the absence of a clear and detailed anatomy of MD activity, with results usually described in terms of large, loosely-defined regions such as “dorsolateral prefrontal cortex”. This lack in precise anatomy is the product of traditional fMRI analysis methods, based on volume-based registration methods in part driven by cortical folds, and the employment of substantial data smoothing that blurs the data. Coupled with the fact that cortical folds vary substantially across individuals, even in twins (Glasser et al., 2016b; Van Essen et al., 2012), and functional areas often do not respect cortical folds (Amunts et al., 2000; Coalson et al., 2018), this has led to significant limitations in relating function to structure in the brain using traditional approaches. Region of interest (ROI) methods can be valuable in identifying individual differences in functional localization, but their definitions are typically based on statistical thresholds that do not necessarily conform to neurobiological criteria. Furthermore, for many questions there are no consensus ROIs, thus limiting comparison and integration of results across studies.

To address these issues, we localized MD activity in relation to the recent state-of-the-art multi-modal Human Connectome Project (HCP) parcellation of human cortex (Glasser et al., 2016a). The HCP cortical parcellation relies on high quality multimodal MRI features (cortical thickness, myelin content, rfMRI connectivity, task fMRI activity), along with surface-based analysis methods (Coalson et al., 2018; Glasser et al., 2016b, 2013) and new areal-feature-based registration algorithms (Robinson et al., 2018, 2014), to parcellate human cortex into 360 regions (180 per hemisphere). Areal delineations were derived from overlapping multi-modal criteria, and areas were named using correspondence with the neuroanatomical literature where possible, bringing a consistent basis in neurobiology and potentially improved comparison with homologous regions in other species.

We analyzed data from 449 HCP subjects, each having a defined individual-specific cortical parcellation. Combining data from 3 task contrasts that tap into working memory, relational reasoning, and arithmetic, we determined which areas show MD properties and examined their functional profiles, patterns of resting state connectivity, and relations to subcortical structures. Our results reveal an extended, largely symmetrical MD network of 27 cortical areas, distributed across frontal, parietal and

temporal lobes. We divide this extended MD system into a core of 10 regions most strongly activated and strongly interconnected, plus a surrounding penumbra, and we relate this functional division to canonical resting state networks also derived from HCP data (Ji et al., 2019). Across the extended MD system, activation profiles for our 3 task contrasts suggest a picture of substantial commonality, modulated by modest but highly significant functional differentiations. MD activation, and strong connectivity with the cortical MD core, are also identified in several subcortical regions. Our results define a highly specific, widely distributed and functionally interconnected MD system, which we suggest forms an integrating core for complex thought and behavior.

Results

We analyzed a cohort of 449 HCP subjects **(for details on data acquisition and preprocessing see Methods sections 1-4).** For our major analysis, each subject's cerebral cortex was parcellated into 360 regions (180 per hemisphere) corresponding to the HCP Multi-Modal Parcellation (MMP) 1.0. Parcellation used an automated classifier to define the borders of each area based on learned features from multiple MRI modalities, including cortical thickness, myelin content, rfMRI connectivity and task fMRI activations **(see Methods section 5)**. Subject-specific parcellation ensured that task and rest fMRI signals extracted from the defined areas would respect individual differences in their sizes, shapes and locations even in the case of subjects with atypical topologic arrangements.

The analysis was based on three suitable fMRI contrasts available in the HCP data: working memory 2-back versus 0-back (WM 2bk>0bk), hard versus easy relational processing (Relational H>E), and math versus story (Math>Story). The first two are standard hard>easy contrasts as commonly used to define MD activity (Duncan and Owen, 2000; Fedorenko et al., 2013). Math>story was added because previous results show a strong MD-like activation pattern associated with arithmetic processing (Amalric and Dehaene, 2017, 2016). For working memory and relational processing, stimuli were visual, whereas for math>story, stimuli were auditory.

Cortical organization of the MD system at the group level

Before considering subject-specific areal analyses, we generated an overview of potential MD areas by calculating a group average MD map. For this, we simply averaged the group average beta maps of the 3 task contrasts and overlaid the resulting combined map on the HCP MMP 1.0 parcellation **(Figure 1a; see also Figure S1 for each contrast separately).** Group average maps were generated by aligning each subject's multi-modal maps using areal-feature-based surface registration **(**MSMAll, Robinson et al 2014; 2018**; see Methods section 4).** MSMAll registration is not substantially driven by cortical folding patterns but instead utilizes myelin and connectivity features to significantly improve the alignment of areas across subjects, with peak probability overlaps reaching >90% for most areas (Coalson et al., 2018)**,** thus allowing us to identify putative areas with MD properties.

Figure 1a shows the resulting overview. To allow a visual comparison, **Figure 1b** shows a previous MD group-average volumetric map, created by the conjunction of 7 hard>easy task contrasts (Fedorenko et al., 2013). Though the two maps are similar, these data emphasize the improved definition obtained with the HCP data and surface-based and areal-feature-based registration methods. On the lateral frontal surface are several clearly distinct activations that show strong bilateral symmetry, with surrounding inactive regions. Tight bands of MD activity are also identifiable in dorsomedial frontal cortex, along the depths of the intraparietal sulcus spreading up to the gyral surface, with an additional restricted region of MD activity in the dorsomedial parietal lobe. The MD region often reported at the occipito-temporal border is also clearly defined in posterior temporal cortex. Even based on these average data, the improved co-registration of the HCP data allows clearer delineation of functional regions, as predicted by Coalson et al., 2018. Rather than broad, fuzzy swaths of MD activity, these data suggest a highly specific but anatomically distributed network of MD regions.

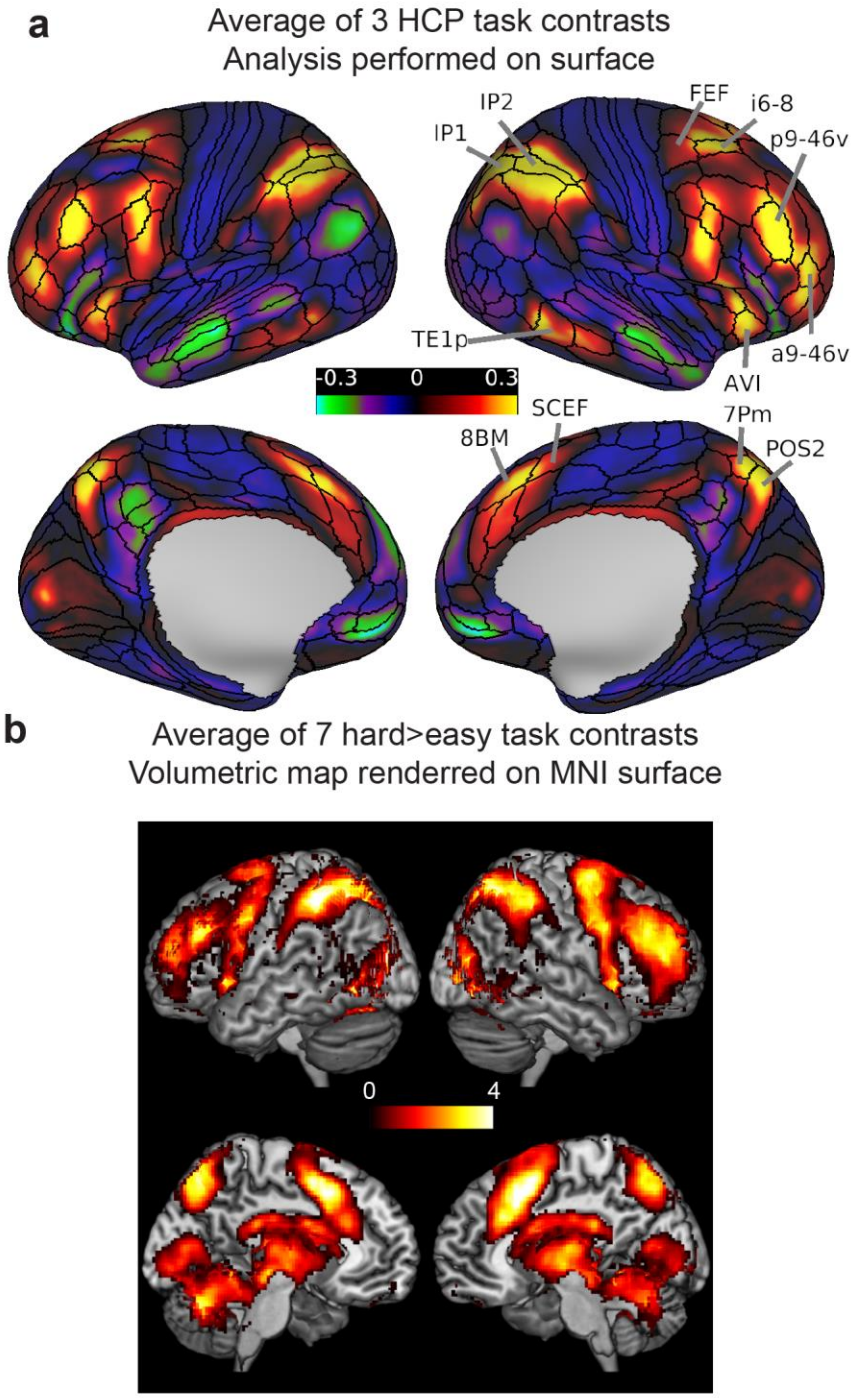

166

167 **Figure 1**. **(a)** Average of the 3 HCP group average task contrasts (WM 2bk>0bk,
168 Relational H>E, Math>Story). Values are beta estimates. Black contours correspond to
169 the HCP multi-modal parcellation MMP_1.0 (210V) areal borders. **(b)** MD map from
170 Fedorenko et al. (2013) computed by averaging 7 hard>easy task contrasts (2mm
171 smoothed). Values are t-statistics. Data available at http://balsa.wustl.edu/XXXX.

Definition of extended and core MD regions using subject-specific cortical parcellation

We next analyzed mean activation values extracted from each subject-specific area. We averaged beta values across vertices within each area, yielding one value per area per subject. For each of our 3 behavioral contrasts, we identified areas with a significant positive difference across the group of 449 subjects ($p<0.05$, Bonferroni corrected for 180 areas)**.** To improve signal-to-noise ratio (SNR), we leveraged the symmetry between hemispheres (see **Figure S2**) and averaged areal activations across hemispheres.

The conjunction of significant areas across the 3 contrasts revealed a set of twenty-seven areas, which we will refer to as the extended MD system **(Figure 2a;** note that average activations from the two hemispheres are projected onto the left**)**. The distribution of the areas closely matches the activations observed in **Figure 1a** and has broad similarity to previous characterizations of MD activity but with substantially improved anatomical precision and several novel findings.

On the dorsal lateral frontal surface, we identify area i6-8 which is immediately anterior to area FEF (a common label given to activations in this region). i6-8 is a newly defined area in the HCP MMP1.0, in the transitional region between classical BA6 and BA8. Localization of MD activity in i6-8, rather than FEF, suggests distinctness from activations driven simply by eye movements in complex tasks. In the HCP MMP1.0, FEF is clearly defined as a distinct area from i6-8 based on several criteria including its anatomical location just anterior to the eye-related portion of the motor cortex and its strong functional connectivity with the LIP/VIP visual complex and the premotor eye field area (PEF) (Glasser et al., 2016).

Near the frontal pole, we identify area a9-46v as a strongly active MD region, separated from the posterior region p9-46v. This separation confirms prior indications of a distinct anterior MD frontal region **(see Figure 1b).** Both a9-46v and p9-46v areas overlap with area 9-46v as delineated cyto-architectonically by Petrides and Pandya (1999) but here are separated into anterior and posterior portions by intervening areas that differ in their myelin and functional connectivity profiles (Glasser et al., 2016). Posterior to p9-46v is a further focus of activity in IFJp, with weaker activity in the surrounding regions 8C and 6r.

In the anterior insula, we identify AVI and an adjacent region of the frontal operculum, FOP5. AVI overlaps with superior portions of the architectonic area Iai of Öngür et al., 2003 (see Glasser et al., 2016). Previous work has attempted to distinguish activity in the anterior insula from the adjacent frontal operculum, with the peak often near the junction of the two (Amiez et al., 2016). In our data, AVI is the more strongly activated.

While previous characterizations of parietal MD activity have focused on the intraparietal sulcus, our results reveal a much more detailed picture, with strongest MD activation in regions of the intraparietal sulcus (IP1, IP2 and PFm), surrounded by the

relatively weaker MD areas dorsally (AIP, LIPd, MIP) and ventrally (PGs). On the dorso-medial parietal surface, data have sometimes hinted at an additional MD region on the dorsomedial surface (see **Figure 1b**). Here we robustly identify the area POS2, a newly defined area in the MMP1.0 that differs from its neighbours in all major multi-modal criteria.

On the lateral surface of the temporal lobe we identify two further areas, TE1m and TE1p. In many previous studies, fronto-parietal MD activity has been accompanied by a similar region of activity in temporo-occipital cortex (e.g. Fedorenko et al., 2013). In many cases, a reasonable interpretation would be higher visual activity, reflecting the visual materials of most imaging studies. In the current study, however, the arithmetic task was auditorily presented, while the other two contrasts were visual, suggesting a genuine MD region.

In **Figure 1a,** the dorso-medial frontal activation spans the border between 8BM/SCEF. In the individual-subject analysis, however, SCEF was not significantly activated across all 3 contrasts. We thus investigated whether the activation indeed spans the border between the two areas. For each subject, we divided each of the two areas into 10 equal segments along their anterior to posterior extent. **Figure 2b** shows that activation in this region starts to build up midway along SCEF, peaks at the border and is sustained throughout 8BM. We then tested whether each segment would survive as an extended MD region on its own. Indeed, all 8BM segments (except for the one most anterior segment on the left hemisphere) survived, whereas only the anterior 2 segments of SCEF were statistically significant **(Figure 2b**; see **Figure S3** for further independent evidence of heterogeneity around the 8BM/SCEF border**)**. Based on these results, for subsequent analyses we combined the statistically significant segments of 8BM and SCEF into a single 'area' labelled 8BM/SCEF.

To further identify the most active areas within the extended MD system, for each contrast we identified areas with activation stronger than the mean across the full set of 27 regions (one sample t-test, $p<0.05$, Bonferroni correction for the 27 extended MD areas). Seven areas were significant in all three contrasts: i6-8, p9-46v, a9-46v, combined 8BM/SCEF area (see below), AVI, IP2 and IP1. Three more areas were significant in two of the three contrasts (**Figure 2c**): IFJp (relational processing and math), 8C and PFm (working memory and relational processing). We refer to this group of areas as the core MD system, with remaining areas of the extended MD system termed the MD penumbra.

Overall, these results identify an extended set of domain-general MD regions. The precise subject-specific areal definitions allowed the identification of several novel areas and improved localization of previously known ones. In the following sections, we further explore the functional properties of core and penumbra regions.

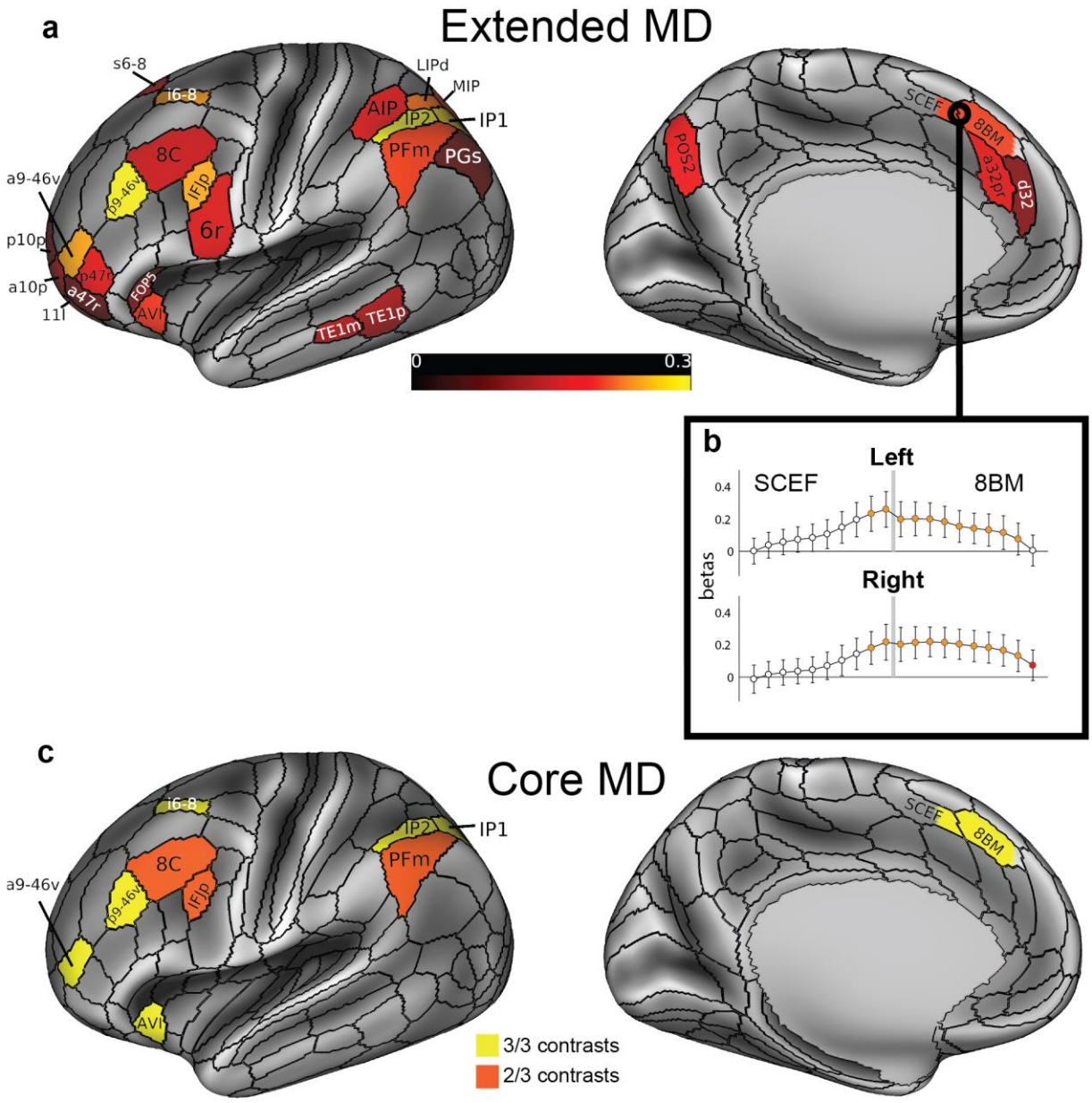

250

251 **Figure 2. (a)** The extended MD system: conjunction of significant areas across 3
252 functional contrasts. Areal colors reflect average betas across the 3 contrasts. Data are
253 averaged across hemispheres, and for illustration projected here onto the left. **(b)**
254 Pattern of activity in regions SCEF (posterior) and 8BM (anterior), divided into posterior
255 to anterior segments. Grey bar indicates 8BM/SCEF border. Orange indicates segments
256 that are part of the extended MD system when activity from both hemispheres is
257 combined (i.e. segments with activity significantly above zero in all 3 behavioral
258 contrasts). Red indicates one additional segment that survives as part of the extended

MD system when activity from each hemisphere is tested separately. **(c)** The core MD system: areas with activity estimates that were significantly higher than the mean activity of all extended MD areas in all 3 contrasts (yellow) and 2 out of 3 contrasts (orange). Data available at http://balsa.wustl.edu/XXXX.

Functional connectivity of the multiple-demand cortex and its relation to resting-state networks

Next we investigated functional connectivity patterns within the MD network and in relation to the rest of the brain using resting state fMRI data (1 hour per subject). A functional connectivity (FC) matrix for each subject was calculated (180x180 areas per hemisphere; full correlation of spatial ICA+FIX and temporal ICA-cleaned time series; **see Methods section 7**). In this analysis, for ease of calculation we retained the original 8BM and SCEF areas, considering only 8BM as core and SCEF as penumbra.

Figure 3a shows the group average connectivity matrix for the extended MD system, separated into core and penumbra. Despite their wide spatial separation, core MD areas show stronger functional connectivity with each other than with the penumbra. To test the robustness of these patterns, for each subject we calculated mean values for 6 different types of cortical connections and compared them using multiple paired sample t-tests **(Figure 3b; see Methods section 7)**. In both hemispheres, functional connectivity between core MD regions was significantly stronger than both their connectivity with the penumbra (left $t(448)= 93.1$, right $t(448)= 79.4$), and the internal penumbra connectivity (left $t(448)= 79.4$, right $t(448)= 66.3$). Mean connectivity of both core and penumbra MD areas with the remainder of the brain were near zero.

We next investigated the spatial similarity between the MD network defined from our conjunction of 3 task contrasts and canonical fMRI resting state networks. For this purpose, we utilized the recent Cole-Anticevic Brain Network Parcellation (CAB-NP) which analyzed resting state data from 337 HCP subjects and identified network communities across HCP MMP1.0 areas (Ji et al., 2019). A comparison of the extended MD and the CAB-NP network parcellation (**Figure 4a)** suggests points of both convergence and divergence. Strikingly, all core MD areas lie within the fronto-parietal network (FPN) of CAB-NP (**Figure 4a**, **top left**). In contrast, penumbra MD areas occupy portions of four networks: FPN, cingulo-opercular network (CON), dorsal attention network (DAN) and the default mode network (DMN) **(Figure 4a, top right).** Importantly, examination of the whole CAB-NP FPN network shows most but not all areas within the MD core or penumbra (left FPN: 10 core, 10 penumbra, 8 non-MD; right FPN: 10 core, 8 penumbra, 4 non-MD) **(Figure 4a, bottom)**.

To emphasize the central role of core MD, we again compared different connectivity subgroups (**Figure 4b;** paired sample t-tests, $p<0.05$, Bonferroni corrected). Within the FPN, we found that connections between core MD regions stand out strikingly in their strength relative to their connectivity with other FPN regions (core-core with core-penumbra: left $t(448)= 60.8$, right $t(448)= 41.6$; and core-core with core-non-MD FPN regions: left $t(448)= 87.7$, right $t(448)= 80.1$). Further within the FPN, core-penumbra connections are stronger than core-non-MD connections (left $t(448)= 57.7$, right $t(448)= 72.4$). Second, we examined connectivity of core MD regions, all lying within FPN, to penumbra and non-MD regions within each of DAN, CON and DMN. The results again highlight a consistent pattern of stronger connectivity between core and penumbra MD

304 regions vs core and non-MD regions within each of the three networks (DAN (left
305 $t(448)= 46.5$, right $t(448)= 41.1$), CON (left $t(448)= 36.3$, right $t(448)= 42.3$) and DMN
306 (left $t(448)= 67.9$, right $t(448)= 86.1$) **(Figure 4b)**.

307 While these results show substantial overlap between MD and FPN – especially for MD
308 core – they also indicate additional structure revealed by the FC data. Connectivity is
309 especially strong between regions within the extended MD system, and strongest
310 between core regions within the canonical FPN. Strong functional connectivity,
311 especially for the core, suggests a suitable architecture for widespread integration of
312 distributed brain states.

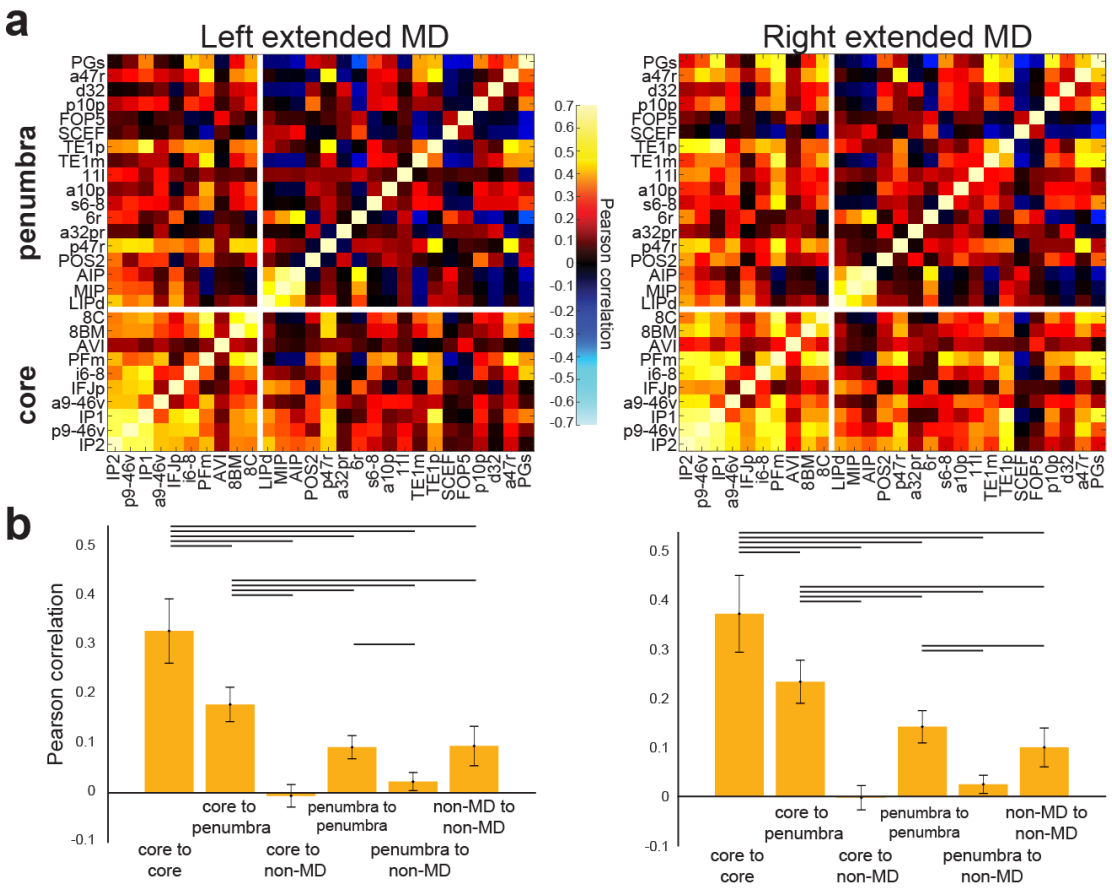

Figure 3. Functional connectivity (FC) of the MD system. **(a)** FC (Pearson correlation) across the MD system. Regions of the extended MD system are separated into core and penumbra, with regions within each set ordered by mean activation (beta) across our 3 functional contrasts. Note the strength of core MD connectivity (lower left box) vs penumbra connectivity (upper right box). **(b)** Statistical comparison (paired sample t-test) between different groups of connections. Lines highlight a statistically significant difference ($p < 0.05$, Bonferroni corrected for 30 comparisons). Data available at http://balsa.wustl.edu/XXXX

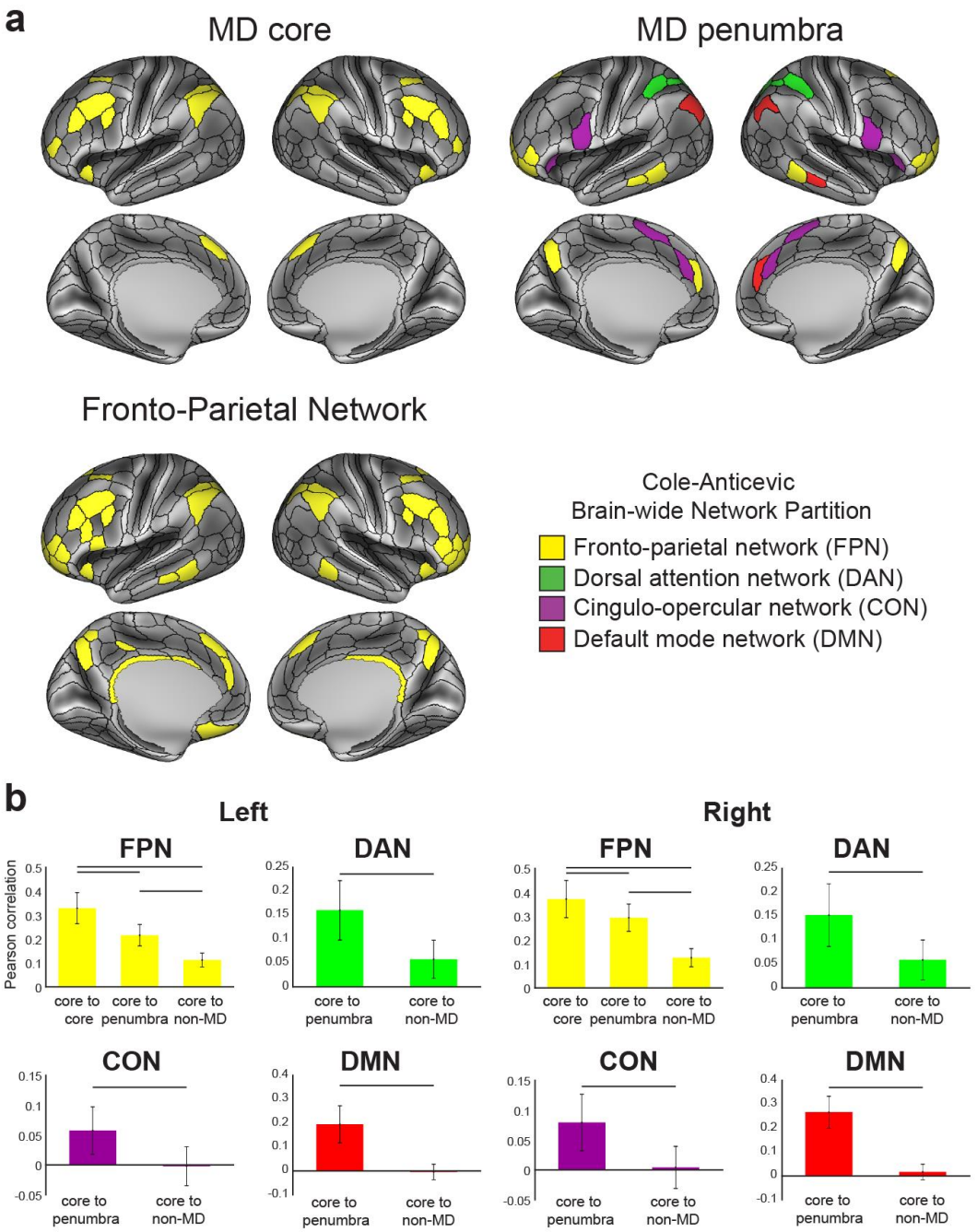

Figure 4. MD system and resting state networks **(a)** Resting state network assignments from the Cole-Anticevic Brain-wide Network Parcellation (CAB-NP; Ji et al., 2018) for the core (left) and penumbra (middle) MD areas, compared to the whole CAB-NP fronto-parietal network (FPN). **(b)** Statistical comparison (paired sample t-test) of connection types for each CAB-NP network. Data available at http://balsa.wustl.edu/XXXX

Task profiles across the multiple-demand cortex

By definition, every MD area showed a significant positive result in each of our 3 behavioral contrasts. Across areas, nevertheless, we explored relative preferences for one contrast over another. To evaluate this quantitatively, **Figure 5a** shows the mean response of each area (averaged across hemispheres) for each contrast. Predominantly, the picture is one of consistency. For nearly all areas, activation was strongest for the math>story contrast, and weakest for hard>easy relational processing. Against this general background, however, there was also differentiation between profiles, with varying patterns of peaks and troughs.

To test the robustness of these patterns, we compared activation profiles in two independent groups of subjects (210P and 210V, the parcellation and validation groups, respectively, used to create the HCP MMP1.0 in Glasser et al., 2016), constructed to avoid shared family membership. As shown in **Figure 5b**, the activation profile for each contrast is almost identical for the two groups. **Figure 5c** quantifies this by correlating activity profiles **(in Figure 5b)** for the two subject groups. Very high correlations on the diagonal ($r > 0.98$) highlight how the precise pattern of activation for a given contrast is very stable when averaged over many individuals. Off-diagonal correlations are much lower ($r=\sim0.5$-0.6). Although all tasks engage all MD areas, there remains considerable and highly consistent inter-areal diversity in precise activation patterns.

To illustrate this inter-areal diversity between the three contrasts, we plotted the normalized profile for each contrast **(line plots in Figure 5d).** For each contrast and each subject, we z-scored activations across MD regions, then averaged the z-scores across subjects. For each region, bar heights **(Figure 5d, bottom)** show the standard deviation of these normalized z-scores across tasks, separately calculated for each subject and then averaged over subjects. Bars were also colored to highlight the relative task preferences (see **Figure 5e**, where the same colors are projected onto the cortical surface).

The results reveal a diversity of relative task preferences across the extended MD network. Relative preference for relational reasoning (green) occurs in a cluster of anterior frontal areas inferior to the core region a9-46v, as well as in 8C. Dorsal frontal regions (e.g. i6-8 and s6-8) show relative preference for working memory, whereas dorsal parietal regions (AIP/LIPd/MIP, and POS2) show relative preference for math. Other relative preferences occur across most regions. Despite relative consistency across the entire extended MD network – with the strongest activation for Math>Story, and weakest for relational processing – there is also clear evidence of relative functional specialization, with each area showing modest but consistent relative preference for one contrast over another.

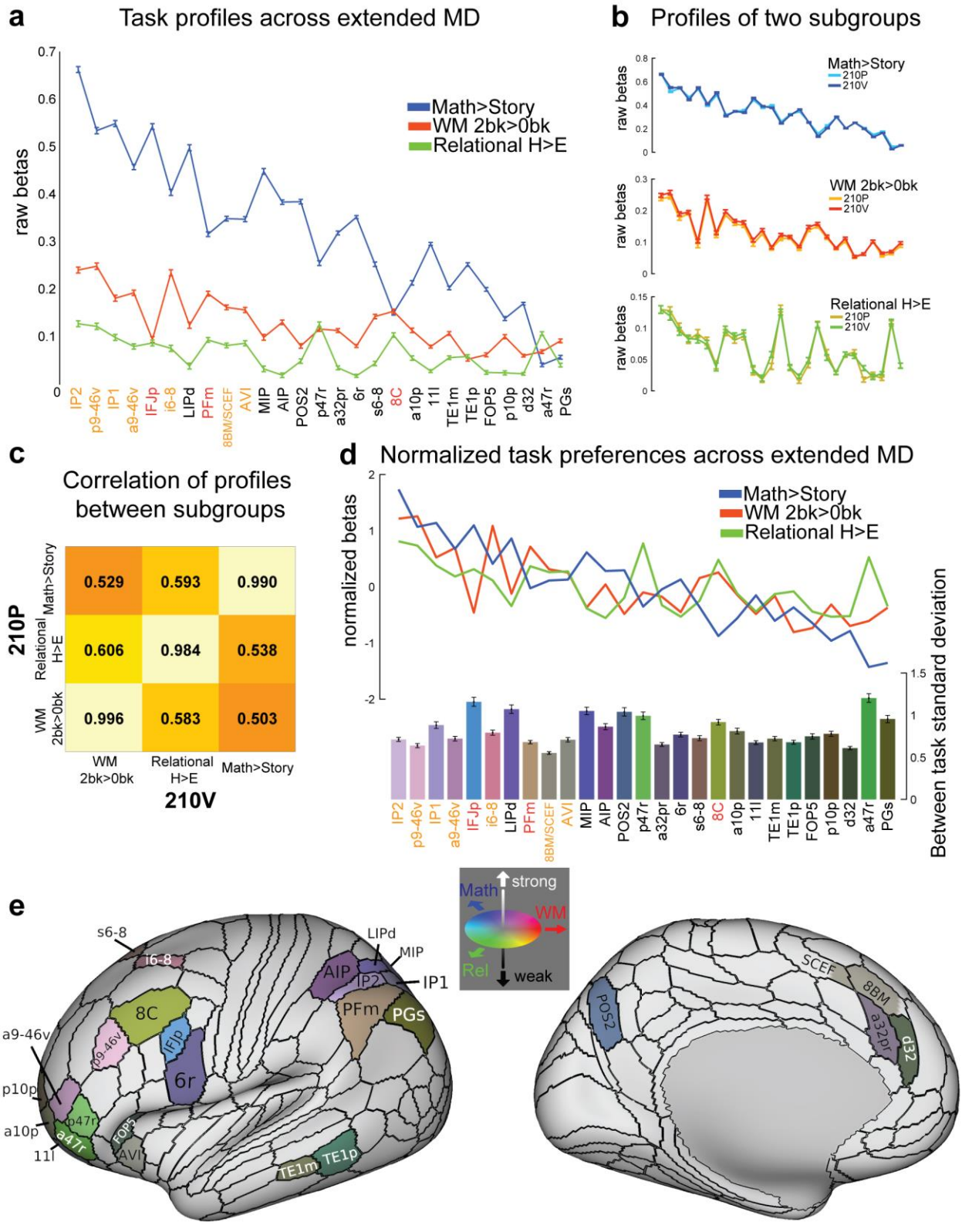

366

Figure 5. Task profiles across the MD system. **(a)** Raw activation estimates (betas) for each contrast. Areas are sorted from left to right according to the strength of their MD response (average across the 3 contrasts). Error bars represent SEM. Core MD areal labels are colored in orange (survived in all 3 contrasts) and red (survived in 2 out of 3 contrasts). **(b)** Task profiles for two independent groups of subjects (210P and 210V). **(c)** Correlation of task profiles between groups. **(d)** Normalized task profiles across the MD system as line plots. Bar heights represent between-task standard deviation, separately calculated for each subject and averaged over subjects. Bar colors indicate relative preferences between tasks. Color wheel indicates red for working memory (WM), green for relational processing (Rel), and blue for math. Intermediate colors show mixed preferences. Brighter and darker colors reflect stronger and weaker MD activation, respectively. **(e)** Cortical projection of the RGB color weighted normalized task profiles. Data available at http://balsa.wustl.edu/XXXX

Subcortical components of the multiple-demand system

To identify the subcortical components of the MD system we used the same 3 behavioral contrasts used for cortical areas. Each subcortical structure was segmented separately for every subject (**see Methods section 4)**, thus avoiding mixing signals from nearby structures or white matter. For each structure, we first identified the significantly activated voxels for each contrast separately (one sample t-test, FDR corrected for each structure separately, $p<0.05$) and then identified the conjunction of significant voxels across the three contrasts. This revealed activation regions bilaterally mainly in the caudate nucleus and cerebellum. Caudate activation peaked in the head and spread into the body **(Figure 6a, left panel)**. Cerebellar activation included separate medial and lateral portions of crus I and II (on dorsal and ventral lateral surface) **(Figure 6a, right panel)**. Activations appear to be largely symmetrical across hemispheres.

We identified two additional small regions in the thalamus bilaterally (antero-medial portion) and the anterior portion of the right globus pallidus **(Figure 6a)**. Interestingly, larger bilateral portions of the thalamus (anterior dorso-medial), putamen (dorso-anterior/mid portion) and globus pallidus (dorso-anterior portion) were significantly activated in only two contrasts (working memory and math) and were deactivated in the relational processing contrast.

In a parallel analysis using resting state data, we aimed to identify the subcortical voxels showing significant functional connectivity with the cortical core MD areas. For this analysis we used the group average dense FC matrix for half of the subjects (210V group) **(see Methods section 7). Figure 6b** shows the statistically significant subcortical voxels (FDR corrected, $p<0.05$). The patterns follow closely the task-identified regions in the caudate nucleus and cerebellum bilaterally. In addition, FC analysis identified significant voxels in bilateral portions of the thalamus (anterior dorso-medial), putamen (dorso-anterior/mid portion) and globus pallidus (dorso-anterior portion), similar to the regions activated in the working memory and math contrasts.

We were able to further compare the MD cerebellar regions with the fronto-parietal network (FPN) identified by resting state data from two studies: Bucker et al 2011 (7 networks parcellation results from 1000 subjects) and CAB-NP (Ji et al., 2018; results from 339 HCP subjects). **Figure 6b (right panel)** illustrates the strong similarity between the FPNs from both studies and the cerebellar MD hotspots in crus I and II.

Due to the lack of individually defined nuclei within each subcortical structure, we measured the degree of overlap between the task vs rest identified MD regions, within each structure, at the group average level. Almost all task-identified MD voxels in caudate, cerebellum and thalamus (except right thalamus) were also detected in the resting state data. Thus, together, task and rest fMRI data converge on identifying a strongly connected subcortical domain related to the cortical MD core.

a Task-identified MD voxels (conjunction of the 3 contrasts)

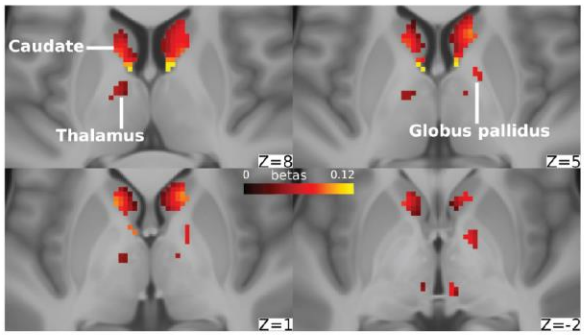

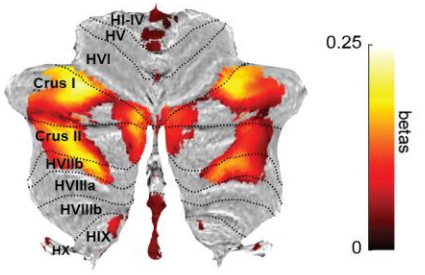

b Rest-identified MD voxels (functional connectivity with cortical MD core)

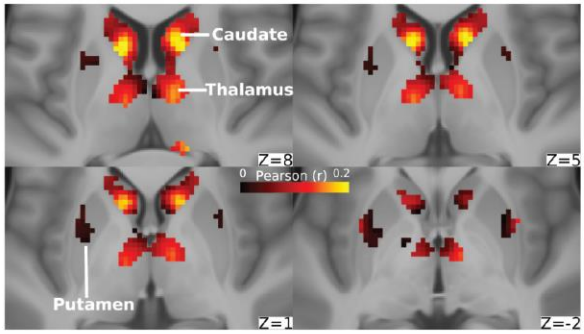

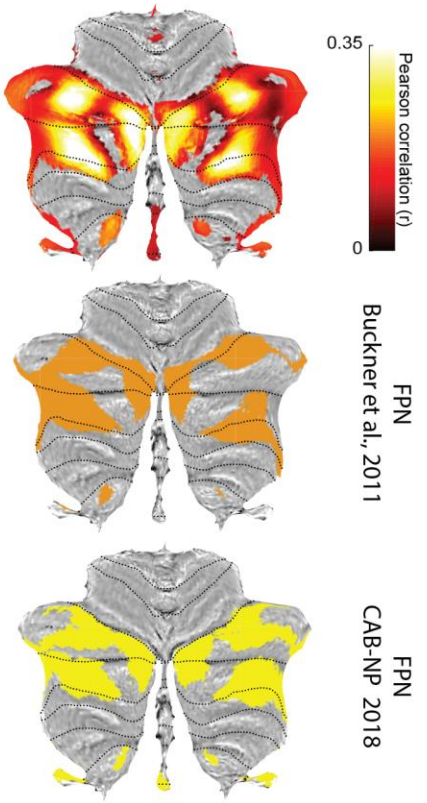

c % MD task voxels identified by rest voxels

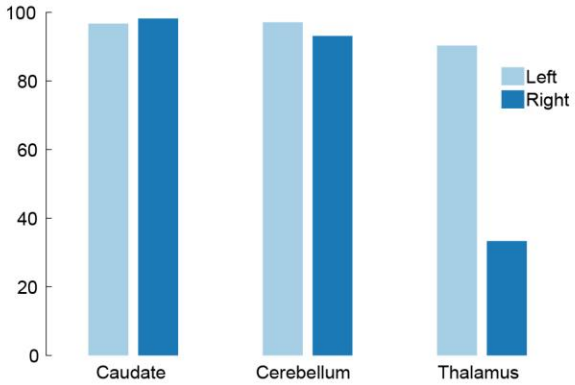

419

Figure 6. Subcortical MD components. **(a)** Left: Conjunction of significant voxels across the three tasks. Right: Cerebellar activity is projected on a flat cerebellum with lines representing anatomical borders (Diedrichsen and Zotow, 2015). **(b)** Left: Subcortical voxels with significant connections to the cortical core MD areas. Right: *(top)* Cerebellar MD connectivity projected on a flat map. *(middle)* FPN from Buckner et al. (2011). *(bottom)* FPN from Ji et al. (2018). **(c)** Percentage of task MD voxels also identified by resting connectivity with MD core. Data available at http://balsa.wustl.edu/XXXX

Discussion

In this study, we used the HCP MMP1.0 cortical parcellation, based on neurobiologically grounded multi-modal MRI features, to demonstrate that diverse cognitive tasks from different sensory modalities engage a widely distributed multiple-demand (MD) network of relatively few areas, in the frontal, parietal and temporal cortices. We identified a set of core regions, characterized by their strong activation and interconnectivity, surrounded by a penumbra, with relatively weaker activations and interconnectivity. We also isolated a set of localized subcortical MD regions, especially in the caudate nucleus and cerebellum, which share strong connectivity with the cortical core MD.

Our use of subject-specific cortical parcellation provides compelling evidence for the existence of highly specific MD regions in the human brain. The improved anatomical precision offered by the HCP methods disclosed novel findings regarding the anatomical and functional organization of the MD network, as well as the functional connectivity of its components.

Why should the brain contain this precise network of MD regions, co-activated during many cognitive activities? On the one hand, MD regions are strongly interconnected, with a widespread and broadly consistent activity profile across tasks. On the other, they are differentiated, with quantitative differences between tasks in precise activity profile. We suggest that this picture is consistent with a system engaged in large-scale integration of brain activity. Within the extended MD system, we propose that the core regions, most strongly active and interconnected, lie at the heart of information integration and exchange. Surrounding penumbra regions, with their connectivity into multiple cortical networks, feed diverse information into the core. Across the entire MD system, co-activation reflects information integration and exchange, while modest functional preferences reflect differential connectivity and information access. Together, these properties allow MD regions, with associated subcortical regions, to build cognitive structures suited to any current task. These proposals are developed and extended in the following sections.

Broad anatomical distribution and relative functional preferences

Our data delineate a highly specific MD network, with core and penumbra components widely distributed across the cortex. Compared to previous data, our results clarify several aspects of this distributed MD pattern.

One such clarification concerns activations in the posterior dorsal prefrontal cortex, often seen in prior work **(see Figure 1b)** in a region close to the FEF. With the increased spatial specificity of the current data, we show that MD activation is localized anterior and dorsal to the FEF, including regions i6-8 (core) and s6-8. These results strongly suggest that MD activation is distinct from activations driven simply by eye movements in complex tasks. Both i6-8 and s6-8 show strongest preference for the WM contrast.

Near the frontal pole, we localized MD activation in one core region (a9-46v) and 5 surrounding penumbra regions. There has been much debate concerning an anterior-posterior gradient of activation on the lateral frontal surface. On the one hand, many tasks produce activation near to the frontal pole, suggesting an MD-like pattern (Ramnani and Owen, 2004). On the other, many studies suggest selective activity in this region, for example associated with abstract reasoning (Bunge et al., 2005; Christoff et al., 2009) or hierarchically-organized cognitive control (Badre, 2008; Badre and Nee, 2018). Our results show that a9-46v is almost as strongly co-activated as more posterior core regions, arguing against a simple gradient of activation. Its adjacent penumbra regions (a47r, p47r) also show clear MD activation but with relative functional preference for the abstract relational reasoning task, matching previous reports of reasoning activation in this region.

The combined 8BM/SCEF MD area on the medial frontal surface showed the least functional preference **(Figure 5d)**. Our findings show MD activation rising to and peaking at the border between 8BM and SCEF, with similar patterns also visible in other task contrasts and fine-grained analysis of functional connectivity **(Figure S3).** In our group-average map, hints of task activation near areal borders can also be seen at the borders of 8C/IFJp and POS2/7Pm **(Figure 1a)**. Though detailed analysis of these functional transitions is beyond our scope here, it is possible that here too MD activation peaks near areal borders. Borders between these areas were defined using robust multiple overlapping functional, architectural and/or topological criteria (Glasser et al., 2016a). Thus, we speculate that our data may reflect close interaction between areas sharing the border, reflecting the general principle of spatial proximity between brain regions that are in close communication.

Previously, many studies have revealed a band of occipito-temporal activation accompanying activation of fronto-parietal MD regions **(see Figure 1b)**. As most tasks used in these studies have been visual, a plausible interpretation might be top-down input into higher visual areas. In our data we identified two penumbra regions, TE1m and TE1p, in posterior temporal cortex. Since these regions were activated by the auditory as well as the visual contrasts, the interpretation of top-down input into higher visual areas is less plausible. The location of these regions midway between higher visual areas, auditory areas and language and sematic areas (Fedorenko et al., 2011; Pobric et al., 2007; Visser et al., 2010) suggests a genuine MD region, situated to integrate higher visual, auditory and semantic/language processing. Similar to previous findings in Broca's area (see Fedorenko et al., 2012), these data highlight an MD area with close proximity to language regions.

Previous studies employing math tasks identify an MD-like pattern that is commonly interpreted as a domain-specific "math network" (Amalric and Dehaene, 2017). Our results show that the math contrast engages all extended MD regions, but with relative preferences among dorsal parietal areas (AIP, LIPd, MIP; and POS2 on the medial

surface) and dorsal frontal region IFJp. We note that in our data, math preferences are potentially confounded with auditory preferences (Michalka et al., 2015).

Very likely, relative functional specializations reflect differential anatomical connections. While putative homologous MD regions in macaques (Mitchell et al., 2016) share many anatomical connections, each also has its own unique fingerprint of connections to and from other brain regions (Markov et al., 2014; Petrides and Pandya, 1999). Acknowledging the current inadequacy of accurate cross-species mapping, these studies portray a picture of a strongly physically interconnected MD system, with its sub regions differentially connected to other brain areas.

On this view, different MD regions are well placed to access different kinds of information. Different tasks, emphasizing different kinds of information lead to partial functional specializations. However, as an integrated cognitive episode is formed, its different contents must be integrated and bound to their functional roles. The rich interconnections between MD regions offer a clear substrate for information exchange and integration.

MD cortex and resting state networks

In this study we identified the extended MD system using a conjunction of three task contrasts. Using MD regions identified from task data, we proceeded to demonstrate strong within-network functional connectivity at rest. As expected, our analysis of resting state data shows much convergence with canonical functional networks derived from the same data (Ji et al., 2019). Within these canonical networks, however, we find additional fine-grained structure. MD core regions constitute a subset of areas within the canonical FPN that are distinguished by especially strong mutual connectivity. This strong connectivity occurs despite wide anatomical separation. In contrast to this core, penumbra regions are distributed across several canonical networks. Again, compared to other regions within those networks, they are distinguished by especially strong connectivity with the MD core. These results support the picture of MD regions as a strong communication skeleton, with penumbra regions in particular drawing together information from several distinct large-scale networks.

This conclusion is reminiscent of extensive recent work using network science approaches (e.g., graph theory) to identify putative cortical communication hubs (Bassett and Sporns, 2017; Bertolero et al., 2018; Petersen and Sporns, 2015; Sporns, 2014). In this graph theoretic approach, hubs are defined by broad connectivity and/or spatial proximity to multiple cortical networks. Typically they include a set of regions resembling the current MD system, but also others including the temporo-parietal junction, extensive regions of the mid- and posterior cingulate and more (Gordon et al., 2018; Power et al., 2013). These connectional findings are broadly consistent with our proposal that MD regions act as an integrative skeleton for cognitive activity, but leave open the question of precise relations between the MD pattern, defined with converging task contrasts, and the definition of hubs based solely on functional connectivity. Because hubs are defined by connectivity with multiple cortical networks, their identification depends on the granularity with which these networks are separated. Such

limitations do not apply to definition of MD regions based on converging task contrasts. Further work may help to contrast the functional role of MD regions relative to hubs defined by connectivity but not showing robust activation across multiple diverse tasks.

Unique connectivity between MD regions can also be revealed by recent work using temporal ICA (tICA), which generates components that are temporally independent (Glasser et al., 2018a; see also Van Essen and Glasser, 2018). We were able to identify at least one rest and one task tICA component with strong spatial similarity (whole brain absolute Pearson correlation r= 0.74 and 0.76 respectively) to the group average MD map from figure 1a (Figure S4). These results demonstrate that the use of automated methods such as tICA has the potential to identify a richer set of brain states, both in rest and task, by imposing temporal but not spatial constraints on the derived components.

Subcortical MD regions

Our data reveal several subcortical MD regions with strong functional connectivity with the cortical MD core. First is the head of the caudate nucleus, also associated with a smaller region in the anterior globus pallidus. In nonhuman primates, the anterior portion of the caudate receives projections from all prefrontal regions (Averbeck et al., 2014). Tracer studies have established that the dorso-lateral prefrontal, dorso-medial prefrontal and parietal cortices, in addition to strong cortico-cortical interconnections, also share converging projections to the caudate, mainly targeting its head, as well as to the globus pallidus (Alexander et al., 1986; Choi et al., 2016; Haber, 2003; Hampson et al., 2006; Kemp and Powell, 1970; Middleton and Strick, 2000; Yeterian and Pandya, 1991). Within the striatum, overlap in the projection zones of nearby cortical areas may in part be mediated by interdigitating dendrites and axons that cross functional boundaries (Averbeck et al., 2014; Haber, 2003). These anatomical findings are consistent with the identified MD activations in the head of the caudate and strongly support its putative role in information integration.

We also identified distributed MD regions in the cerebellum. Tracer studies identify polysynaptic connections between the prefrontal cortex and the lateral portions of crus I and II as well as vermal lobules VII and IX (see Buckner, 2013 and Ramnani, 2006), largely overlapping with our MD cerebellar regions. In addition, previous studies have implicated similar cerebellar regions in several aspects of complex cognitive activity (King et al., 2018) as well as encoding task-relevant information (Balsters et al., 2013). Importantly, MD cerebellar regions do not overlap with motor-related regions (Diedrichsen and Zotow, 2015). Not surprisingly, there is strong overlap between the cerebellar regions identified here, by converging task contrasts and strong connectivity to the MD cortical core, and the FPN-related cerebellar network defined in previous studies (Buckner et al., 2011; Ji et al., 2019). Importantly, the cerebellar MD regions were identified by connections with the more spatially restricted cortical MD core in comparison with the cortical FPN, further suggesting a central role for the cortical MD core.

We also identified putative MD regions in the anterior portion of the thalamus. In this case, small regions identified from our conjunction of task contrasts compare with a larger region identified using resting state connectivity. The connectivity identified thalamic regions are in line with the findings of numerous studies reporting strong anatomical and functional connectivity between thalamic nuclei (especially medio-dorsal portions) and fronto-parietal cortices (Haber, 2003; Halassa and Kastner, 2017). The notably small task-identified parietal MD region reflects deactivation of the majority of parietal cortex in relational reasoning.

Further work at higher field MRI strength (e.g., 7T) may help clarify the role of these and other subcortical regions associated with the cortical MD system. Meanwhile, in agreement with known anatomy, our data suggest extensive cortical-subcortical interaction in control of complex cognitive activity.

Creating the structure of complex cognition

In behavior and thought, the richness of even a simple cognitive event, and the precise relations that must be established between different components of that event, call for a widely-connected system, able to access any kind of cognitive content. Our data highlight several properties that suit the MD system to construct complex cognitive episodes. The MD system is made up of regions that are widely dispersed anatomically, yet tightly functionally connected and co-recruited by tasks of many different kinds. Our data identify a core, with the strongest pattern of widespread recruitment and connectivity, supported by a surrounding penumbra.

Owing to their differential anatomical and functional connections, different MD regions may be preferentially recruited during tasks with different contents. However, their strong interconnectedness likely allow different information to become quickly integrated and exchanged, leading to a dominant pattern of co-activation. Extensive MD connections to other regions also suggest a broad role in coordinating brain activity in service of the task at hand. This proposal conforms with the finding that the MD system, among different brain networks, is the most striking in changing its global brain connectivity during different task states (Cole et al., 2013).

The ability of the MD system to dynamically and broadly represent many kinds of information is supported by numerous human fMRI studies employing multi-variate pattern analysis (MVPA), as well as electrophysiological studies in animals (Miller and Cohen, 2001; Stokes et al., 2013; see Woolgar et al., 2016 for a comprehensive review of MVPA studies). In putative monkey MD regions, many studies identify neurons with mixed selectivity, allowing integration of specific stimuli and specific task contexts (Genovesio et al., 2016; Naya et al., 2017; Parthasarathy et al., 2017; Rigotti et al., 2013; Stokes et al., 2013). Conjunctive coding/mixed selectivity is likely critical in assembling the correct structured relations between the component parts of a cognitive episode (Duncan, 2013; Rigotti et al., 2013).

For cumulative progress in understanding brain activity, a basic step is definition of an accepted set of component regions. In the case of MD activity, progress has been slow because we lack such a precise definition, leading to many thousands of studies showing similar activity patterns, but little agreement over questions such as functional similarity/differentiation. Based on the HCP multi-modal parcellation, our work defines a precise network of core MD regions and their surrounding penumbra, and establishes a pattern of widespread co-recruitment, relative functional differentiation, and strong connectivity. Precisely specified MD regions provide a basis for detailed functional investigation, cross-reference between studies, and identification of cross-species homologs. With these results, we lay the groundwork for a new phase in understanding one of the brain's most important, best-known but least understood functional networks.

Methods

1. Subjects

The analyzed dataset consisted of 449 healthy volunteers from the Human Connectome Project (HCP) S500 release. Subjects were recruited from Washington University (St. Louis, MO) and the surrounding area (186 males, 263 females, with age ranges (22-25 n=69; 26-30 n=208; 31-35 n= 169; 36+ n=3). Informed consent was obtained from each subject as approved by the institutional review board at Washington University at St. Louis.

2. Image Acquisition

MRI acquisition protocols have been previously described (Glasser et al., 2013; Smith et al., 2013; Uğurbil et al., 2013). All 449 subjects underwent the following scans: structural (at least one T1w and one T2w scan), rfMRI (4 runs X 15 minutes), and task fMRI (7 tasks, 46.6 minutes total). Images were acquired using a customized 3T Siemens 'Connectom' scanner having a 100mT/m SC72 gradient insert and using a standard Siemens 32-channel RF receive head coil. At least one 3D T1w MPRAGE and one 3D T2w SPACE image were acquired at 0.7 mm isotropic resolution. Whole brain rfMRI and task fMRI data were acquired using identical multi-band EPI sequence parameters of 2 mm isotropic resolution with a TR=720 ms. Spin echo phase reversed images were acquired during the fMRI scanning sessions to enable accurate cross-modal registrations of the T2w and fMRI images to the T1w image in each subject (standard dual gradient echo fieldmaps were acquired to correct T1w and T2w images for readout distortion). Additionally, the spin echo field maps acquired during the fMRI session (with matched geometry and echo spacing to the gradient echo fMRI data) were used to compute a more accurate fMRI bias field correction and to segment regions of gradient echo signal loss.

3. Task Paradigms

Each subject performed 7 tasks in the scanner over two sessions. In the current study we analyzed data from 3 tasks: working memory (performed in session 1), math/language and relational processing (performed in session 2). Subjects performed 2 runs of each task. The following task details are adapted from Barch et al. (2013) on HCP fMRI tasks.

Working Memory: Each run consisted of 8 task blocks (10 trials of 2.5 s each, for 25 s) and 4 fixation blocks (15 s each). Within each run, 4 blocks used a 2-back working memory task (respond 'target' whenever the current stimulus was the same as the one two back) and the other 4 used a 0-back working memory task (a target cue was presented at the start of each block, and a 'target' response was required to any presentation of that stimulus during the block). A 2.5 s cue indicated the task type (and target for 0-back) at the start of the block. On each trial, the stimulus was presented for 2 s, followed by a 500 ms ITI. In each block there were 2 targets, and (in the case of the

2-back task) 2–3 non-target lures (repeated items in the wrong n-back position, either 1-back or 3-back). Stimuli consisted of pictures of faces, places, tools and body parts; within each run, the 4 different stimulus types were presented in separate blocks. Subjects had to respond to non-targets using a middle finger press and to targets using an index finger press.

Math/language: Each run consisted of 4 blocks of a math task interleaved with 4 blocks of a story task. The lengths of the blocks varied (average of approximately 30 s), but the task was designed so that the math task blocks matched the length of the story task blocks, with some additional math trials at the end of the task to complete the 3.8 min run as needed. The math task required subjects to complete addition and subtraction problems, auditorily presented. Each trial had a problem of the form "X + Y =" or "X – Y =", followed by two choices. The subjects pushed a button to select either the first or the second answer. Problems were adapted to maintain a similar level of difficulty across subjects. The story blocks presented subjects with brief auditory stories (5–9 sentences) adapted from Aesop's fables, followed by a 2-alternative forced choice question that asked the subjects about the topic of the story. The example provided in the original Binder paper (p. 1466) is "For example, after a story about an eagle that saves a man who had done him a favor, subjects were asked, 'That was about revenge or reciprocity?'". For more details on the task, see Binder et al. (2011).

Relational Processing: Stimuli were drawn from a set of 6 different shapes filled with 1 of 6 different textures. In the hard condition, subjects were presented with 2 pairs of objects, with one pair at the top of the screen and the other pair at the bottom of the screen. They were told that they should first decide what dimension(s) differed across the top pair of objects (shape or texture) and then they should decide whether the bottom pair of objects also differed along the same dimension(s) (e.g., if the top pair differs only in shape, does the bottom pair also differ only in shape?). In the easy condition, subjects were shown two objects at the top of the screen and one object at the bottom of the screen, and a word in the middle of the screen (either "shape" or "texture"). They were told to decide whether the bottom object matched either of the top two objects on that dimension (e.g., if the word is "shape", is the bottom object the same shape as either of the top two objects?). For the hard condition, stimuli were presented for 3500 ms, with a 500 ms ITI, with four trials per block. In the easy condition, stimuli were presented for 2800 ms, with a 400 ms ITI, with 5 trials per block. Each type of block (hard or easy) lasted a total of 18 s. In each of the two runs of this task, there were 3 hard blocks, 3 easy blocks and 3 16 s fixation blocks.

4. Data preprocessing

Data were preprocessed using the HCP's minimal preprocessing pipelines (Glasser et al., 2013). Briefly, for each subject, structural images (T1w and T2w) were corrected for spatial distortions and used for accurate extraction of cortical surfaces and subcortical structures. To align subcortical structures across subjects, structural images were

719 registered using non-linear volume registration to Montreal Neurological Institute (MNI)
720 space.

721 Functional images (rest and task) were corrected for spatial distortions, motion
722 corrected, and mapped from volume to surface space using ribbon-constrained volume
723 to surface mapping. Subcortical data were also projected to the set of extracted
724 subcortical structure voxels and combined with the surface data to form the standard
725 CIFTI grayordinates space. Data were smoothed by a 2mm FWHM kernel in the
726 grayordinate space that avoids mixing data across gyral banks for surface data and
727 avoids mixing areal borders for subcortical data. Rest and task fMRI data were
728 additionally identically cleaned up for spatially specific noise using spatial ICA+FIX
729 (Salimi-Khorshidi et al., 2014) and global structured noise using temporal ICA (Glasser
730 et al., 2018).

731 For accurate cross-subject registration of cortical surfaces, a multi-modal surface
732 matching (MSM) algorithm (Robinson et al., 2014) was used to optimize the alignment
733 of cortical areas based on features from different modalities. MSMSulc ('sulc': cortical
734 folds average convexity) was used to initialize MSMAll, which then utilized myelin,
735 resting state network (RSN) and rfMRI visuotopic maps. Myelin maps were computed
736 using the ratio of T1w/T2w images (Glasser et al., 2014; Glasser and Van Essen, 2011).
737 Individual subject RSN maps were calculated using a weighted regression method
738 (Glasser et al., 2016a).

739 **5. HCP multi-modal parcellation and areal classifier**

740 The HCP multi-modal parcellation map (MMP) 1.0 (Glasser et al., 2016) was first
741 created using a semi-automated approach utilizing the group average maps of multiple
742 modalities (cortical thickness, myelin, resting state functional connectivity, and task
743 activations). For each modality, the gradient was computed as the 1st spatial derivative
744 along the cortical surface; ridges were local regions with the highest value and thus the
745 most sudden change in a feature. Overlapping gradient ridges across modalities were
746 used to draw putative areal borders with manual initialization and algorithmic
747 refinement. Defined areas were reviewed by neuroanatomists, compared whenever
748 possible to previously identified areas in the literature, and labelled. This resulted in
749 defining 180 areas per hemisphere. A multi-modal areal classifier was then developed
750 for automated definition of areas in each subject using the multi-modal feature maps.
751 The classifier was trained, tested and validated on independent groups of subjects from
752 the same 449 cohort used in this study (Glasser et al., 2016a).

753 **6. Task fMRI analysis**

754 Task fMRI analysis steps are detailed in Barch et al. (2013). Briefly, autocorrelation was
755 estimated using FSL's FILM on the surface. Activity estimates were computed for the
756 preprocessed functional time series from each run using a general linear model (GLM)
757 implemented in FSL's FILM (Woolrich et al., 2001). For the *working memory* task, 8
758 regressors were used - one for each type of stimulus in each of the N-back conditions.

Each predictor covered the period from the onset of the cue to the offset of the final trial (27.5 s). For the *math* task, 2 regressors were used. The math regressor covered the duration of a set of math questions designed to roughly match the duration of the story blocks. The story regressor covered the variable duration of a short story, question, and response period (~30 s). For the *relational processing* task, two regressors were used, each covering the duration of 18 s composed of four trials for the hard condition and five trials for the easy condition. In each case, linear contrasts of these predictors were computed to estimate effects of interest: WM 2bk>0bk, Relational H>E, and Math>Story.

All regressors were convolved with a canonical hemodynamic response function and its temporal derivative. The time series and the GLM design were temporally filtered with a Gaussian-weighted linear highpass filter with a cutoff of 200 seconds. Finally, the time series was prewhitened within FILM to correct for autocorrelations in the fMRI data. Surface-based autocorrelation estimate smoothing was incorporated into FSL's FILM at a sigma of 5mm. Fixed-effects analyses were conducted using FSL's FEAT to estimate the average effects across runs within each subject.

For further analysis of effect sizes, beta 'cope' maps was performed using custom built MATLAB scripts after moving the data from the CIFTI file format to the MATLAB workspace. Activity estimates on the surface vertices were averaged across vertices that shared the same areal label for each subject. Unless mentioned otherwise, parametric statistical tests (one-sample and paired sample t-tests) were used.

7. rfMRI Functional connectivity analysis

For each subject, a 'parcellated' FC map was computed by averaging the time series across cortical vertices that shared the same areal label and correlating the average time series giving a 360x360 FC matrix for each subject.

For comparison of connection types (Figure 3b, d), connectivities for each subject were simply averaged across each group of areas following r-to-z transformation.

For subcortical analysis, the group average dense FC map for the 210V subjects group was used for the identification of subcortical voxels. For each subcortical voxel, an average connectivity to the cortical MD core was obtained by first calculating connectivity to each core area (after averaging across each area's vertices), and then averaging these connectivities following r-to-z transformation. A permutation testing approach (100,000 permutations) was used to identify the significant voxels by building a null distribution for each voxel based on its FC estimate to sets of 10 random brain areas. A voxel was determined as significantly connected to the MD system when its FC estimate was in the top 97.5^{th} percentile.

Data availability. [upon acceptance] Data used for generating each of the imaging-based figures [will be] made available by the BALSA database. Selecting the URL at the end of each figure will link to a BALSA page that allows downloading of a scene file plus associated data files; opening the scene file in Connectome Workbench will recapitulate the exact configuration of data and annotations as displayed in the figure.

Acknowledgments

Data were provided by the Human Connectome Project. We would like to thank Michael Cole and Alan Anticevic for sharing their network parcellation data before it was published. We would like to thank Daniel Mitchell for sharing the MD volumetric map. J.D. is supported by MRC grant SUAG/002/RG91365. D.C.V.E is supported by NIH grant RO1 MH-60974. M.A. is supported by a Cambridge Commonwealth European and International Trust – Yousef Jameel scholarship.

Author Contributions (CRediT taxonomy)

Conceptualization, J.D., M.A.; Methodology, M.A, J.D., M.F.G, D.C.V.E; Formal Analysis, M.A., M.F.G; Writing – original draft, M.A, J.D.; Writing – Review & Editing M.A, J.D., M.F.G, D.C.V.E

Declaration of interests

The authors declare no competing interests.

Supplementary Figures

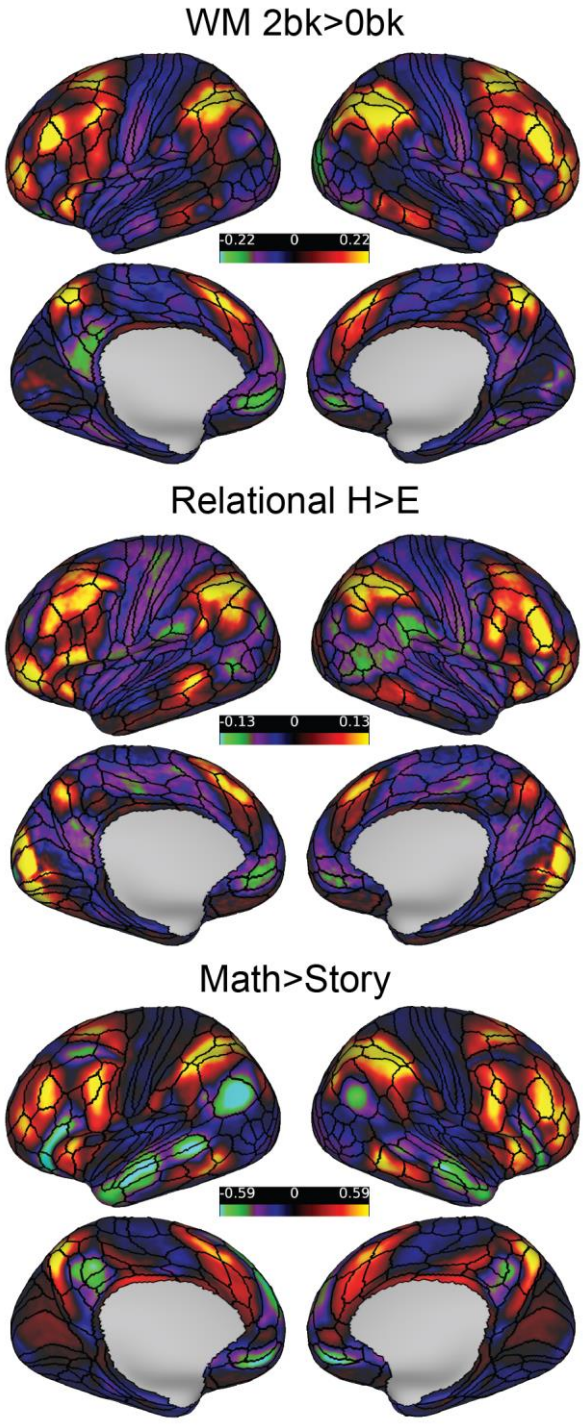

Figure S1. Contrast maps for each task.

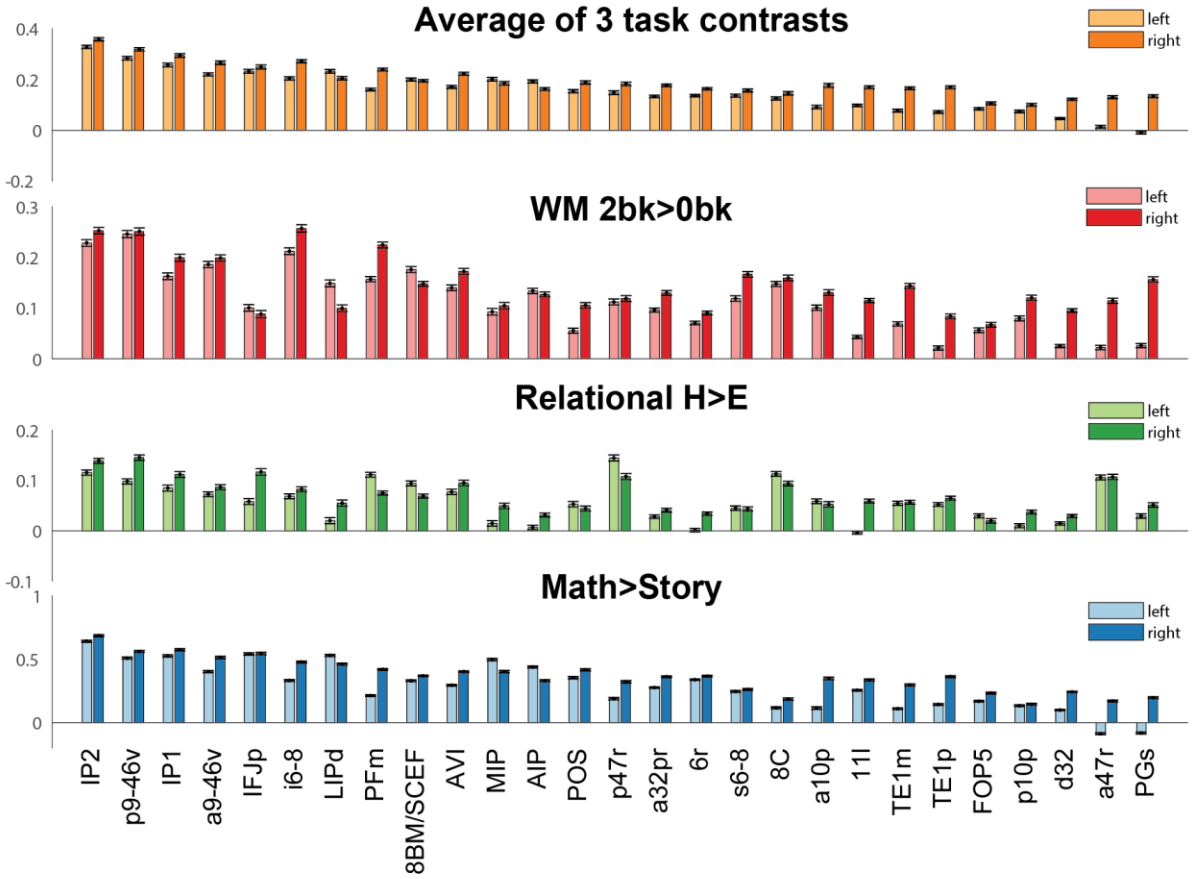

Figure S2. Extended MD for each hemisphere. Group average responses for the MD areas of both hemispheres. First row: average of the 3 HCP contrasts. Second row: Working memory. Third row: Relational reasoning. Fourth row: Math>story. Error bars are SEMs.

824

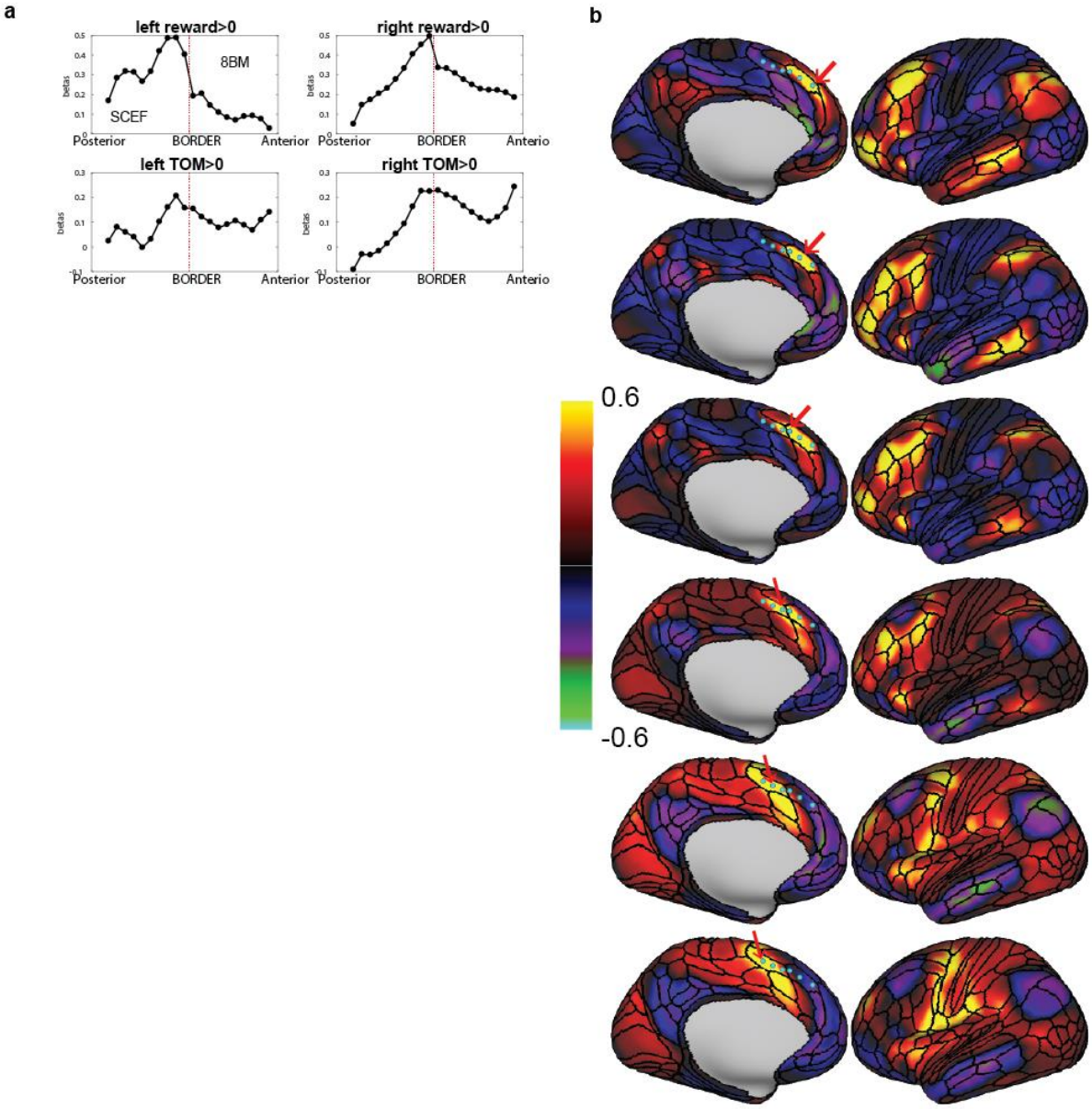

825

826 **Figure S3. 8BM/SCEF border. (a)** Group average responses for two HCP contrasts
827 across the 8BM/SCEF border, Reward>Baseline and Theory of Mind (TOM)>Baseline,
828 showing a similar pattern of build up within SCEF reaching a peak near the 8BM/SCEF
829 border. **(b)** Functional connectivity maps for seeds (210V map, left hemisphere) along
830 an antero-posterior gradient for the left 8BM/SCEF areas. Arrows mark the seed related
831 to each column's maps. Note how the seed in row 4 is in SCEF near the 8BM/SCEF
832 border and still shows an MD like connectivity pattern, especially the strong connectivity
833 to i6-8. More posterior seeds in SCEF show a markedly different pattern with strong
834 connectivity to FEF. Color scale is Pearson correlation (r).

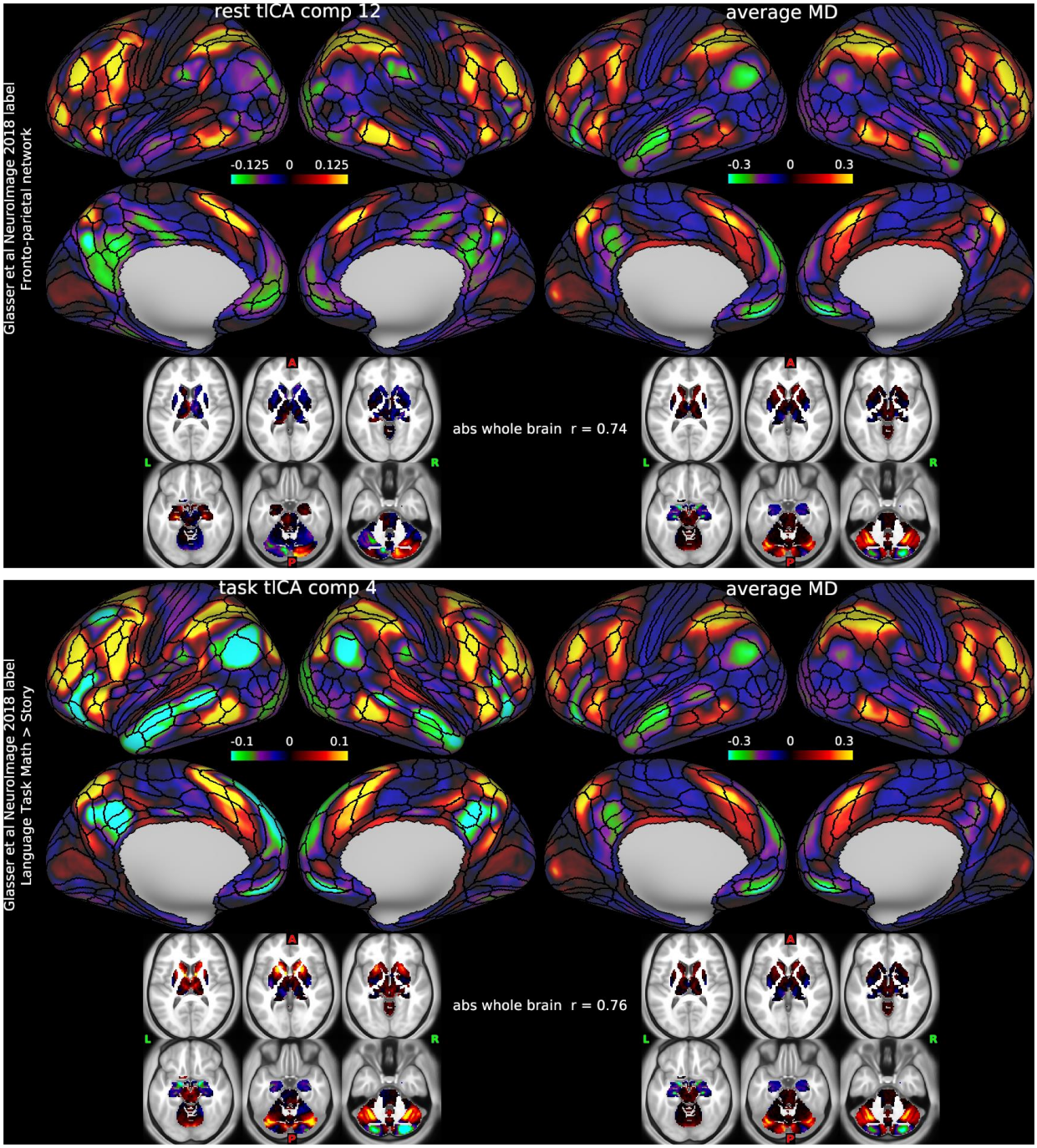

Figure S4. MD and temporal ICA. Most correlated temporal ICA components (from Glasser et al., 2018a) with MD average map. Top: rest tICA component 12. Bottom: task tICA component 4.

References

Alexander GE, DeLong MR, Strick PL. 1986. Parallel Organization of Functionally Segregated Circuits Linking Basal Ganglia and Cortex. *Annu Rev Neurosci* **9**:357–381. doi:10.1146/annurev.ne.09.030186.002041

Amalric M, Dehaene S. 2017. Cortical circuits for mathematical knowledge: evidence for a major subdivision within the brain's semantic networks. *Philos Trans R Soc B Biol Sci* **373**:20160515. doi:10.1098/rstb.2016.0515

Amalric M, Dehaene S. 2016. Origins of the brain networks for advanced mathematics in expert mathematicians. *Proc Natl Acad Sci* **113**:4909–4917. doi:10.1073/pnas.1603205113

Amiez C, Wutte MG, Faillenot I, Petrides M, Burle B, Procyk E. 2016. Single subject analyses reveal consistent recruitment of frontal operculum in performance monitoring. *Neuroimage* **133**:266–278. doi:10.1016/j.neuroimage.2016.03.003

Amunts K, Malikovic A, Mohlberg H, Schormann T, Zilles K. 2000. Brodmann's Areas 17 and 18 Brought into Stereotaxic Space—Where and How Variable? *Neuroimage* **11**:66–84. doi:10.1006/nimg.1999.0516

Averbeck BB, Lehman J, Jacobson M, Haber SN. 2014. Estimates of Projection Overlap and Zones of Convergence within Frontal-Striatal Circuits. *J Neurosci* **34**:9497–9505. doi:10.1523/JNEUROSCI.5806-12.2014

Badre D. 2008. Cognitive control, hierarchy, and the rostro–caudal organization of the frontal lobes. *Trends Cogn Sci* **12**:193–200. doi:10.1016/j.tics.2008.02.004

Badre D, Nee DE. 2018. Frontal Cortex and the Hierarchical Control of Behavior. *Trends Cogn Sci* **22**:170–188. doi:10.1016/j.tics.2017.11.005

Balsters JH, Whelan CD, Robertson IH, Ramnani N. 2013. Cerebellum and Cognition: Evidence for the Encoding of Higher Order Rules. *Cereb Cortex* **23**:1433–1443. doi:10.1093/cercor/bhs127

Barch DM, Burgess GC, Harms MP, Petersen SE, Schlaggar BL, Corbetta M, Glasser MF, Curtiss S, Dixit S, Feldt C, Nolan D, Bryant E, Hartley T, Footer O, Bjork JM, Poldrack R, Smith S, Johansen-Berg H, Snyder AZ, Van Essen DC. 2013. Function in the human connectome: Task-fMRI and individual differences in behavior. *Neuroimage* **80**:169–189. doi:10.1016/j.neuroimage.2013.05.033

Bassett DS, Sporns O. 2017. Network neuroscience. *Nat Neurosci* **20**:353–364. doi:10.1038/nn.4502

Bertolero MA, Yeo BTT, Bassett DS, D'Esposito M. 2018. A mechanistic model of connector hubs, modularity and cognition. *Nat Hum Behav* **2**:765–777. doi:10.1038/s41562-018-0420-6

Buckner RL. 2013. The cerebellum and cognitive function: 25 years of insight from anatomy and neuroimaging. *Neuron* **80**:807–815. doi:10.1016/j.neuron.2013.10.044

878 Buckner RL, Krienen FM, Castellanos A, Diaz JC, Yeo BTT. 2011. The organization of
879 the human cerebellum estimated by intrinsic functional connectivity. *J Neurophysiol*
880 **106**:2322–2345. doi:10.1152/jn.00339.2011.

881 Bunge SA, Wendelken C, Badre D, Wagner AD. 2005. Analogical reasoning and
882 prefrontal cortex: evidence for separable retrieval and integration mechanisms.
883 *Cereb Cortex* **15**:239–49. doi:10.1093/cercor/bhh126

884 Choi EY, Tanimura Y, Vage PR, Yates EH, Haber SN. 2016. Convergence of prefrontal
885 and parietal anatomical projections in a connectional hub in the striatum.
886 *Neuroimage* **146**:821–832. doi:10.1016/j.neuroimage.2016.09.037

887 Christoff K, Keramatian K, Gordon AM, Smith R, Mädler B. 2009. Prefrontal
888 organization of cognitive control according to levels of abstraction. *Brain Res*
889 **1286**:94–105. doi:10.1016/j.brainres.2009.05.096

890 Coalson TS, Essen DC Van, Glasser MF. 2018. The impact of traditional neuroimaging
891 methods on the spatial localization of cortical areas. *Proc Natl Acad Sci*
892 **115**:E6356–E6365. doi:10.1073/PNAS.1801582115

893 Cole MW, Reynolds JR, Power JD, Repovs G, Anticevic A, Braver TS. 2013. Multi-task
894 connectivity reveals flexible hubs for adaptive task control. *Nat Neurosci* **16**:1348–
895 1355. doi:10.1038/nn.3470

896 Cole MW, Schneider W. 2007. The cognitive control network: Integrated cortical regions
897 with dissociable functions. *Neuroimage* **37**:343–360.
898 doi:10.1016/j.neuroimage.2007.03.071

899 Dehaene S, Kerszberg M, Changeux J-P. 1998. A neuronal model of a global
900 workspace in effortful cognitive tasks. *Proc Natl Acad Sci* **95**:14529–14534.
901 doi:10.1073/pnas.95.24.14529

902 Desimone R, Duncan J. 1995. Neural mechanisms of selective visual attention. *Annu*
903 *Rev Neurosci* **18**:193–222. doi:10.1146/annurev.ne.18.030195.001205

904 Diedrichsen J, Zotow E. 2015. Surface-based display of volume-averaged cerebellar
905 imaging data. *PLoS One* **10**:1–18. doi:10.1371/journal.pone.0133402

906 Duncan J. 2013. The Structure of Cognition: Attentional Episodes in Mind and Brain.
907 *Neuron* **80**:35–50. doi:10.1016/j.neuron.2013.09.015

908 Duncan J. 2010. The multiple-demand (MD) system of the primate brain: mental
909 programs for intelligent behaviour. *Trends Cogn Sci* **14**:172–179.
910 doi:10.1016/j.tics.2010.01.004

911 Duncan J. 2006. EPS Mid-Career Award 2004: Brain mechanisms of attention. *Q J Exp*
912 *Psychol* **59**:2–27. doi:10.1080/17470210500260674

913 Duncan J. 2001. An adaptive coding model of neural function in prefrontal cortex. *Nat*
914 *Rev Neurosci* **2**:820–829. doi:10.1038/35097575

915 Duncan J, Burgess P, Emslie H. 1995. Fluid intelligence after frontal lobe lesions.

Neuropsychologia **33**:261–268. doi:10.1016/0028-3932(94)00124-8

Duncan J, Owen AM. 2000. Common regions of the human frontal lobe recruited by diverse cognitive demands. *Trends Neurosci* **23**:475–483. doi:10.1016/S0166-2236(00)01633-7

Fedorenko E, Behr MK, Kanwisher N. 2011. Functional specificity for high-level linguistic processing in the human brain. *Proc Natl Acad Sci U S A* **108**:16428–16433. doi:10.1073/pnas.1

Fedorenko E, Duncan J, Kanwisher N. 2013. Broad domain generality in focal regions of frontal and parietal cortex. *Proc Natl Acad Sci U S A* **110**:16616–21. doi:10.1073/pnas.1315235110

Fedorenko E, Duncan J, Kanwisher N. 2012. Language-selective and domain-general regions lie side by side within Broca's area. *Curr Biol* **22**:2059–2062. doi:10.1016/j.cub.2012.09.011

Ford KA, Gati JS, Menon RS, Everling S. 2009. BOLD fMRI activation for anti-saccades in nonhuman primates. *Neuroimage* **45**:470–476. doi:10.1016/j.neuroimage.2008.12.009

Fusi S, Miller EK, Rigotti M. 2016. Why neurons mix: High dimensionality for higher cognition. *Curr Opin Neurobiol*. doi:10.1016/j.conb.2016.01.010

Genovesio A, Seitz LK, Tsujimoto S, Wise SP. 2016. Context-Dependent Duration Signals in the Primate Prefrontal Cortex. *Cereb Cortex* **26**:3345–3356. doi:10.1093/cercor/bhv156

Glascher J, Rudrauf D, Colom R, Paul LK, Tranel D, Damasio H, Adolphs R. 2010. Distributed neural system for general intelligence revealed by lesion mapping. *Proc Natl Acad Sci* **107**:4705–4709. doi:10.1073/pnas.0910397107

Glasser MF, Coalson TS, Bijsterbosch JD, Harrison SJ, Harms MP, Anticevic A, Van Essen DC, Smith SM. 2018. Using temporal ICA to selectively remove global noise while preserving global signal in functional MRI data. *Neuroimage* **181**:692–717. doi:10.1016/j.neuroimage.2018.04.076

Glasser MF, Coalson TS, Robinson EC, Hacker CD, Harwell J, Yacoub E, Ugurbil K, Andersson J, Beckmann CF, Jenkinson M, Smith SM, Van Essen DC. 2016a. A multi-modal parcellation of human cerebral cortex. *Nat Publ Gr* **536**. doi:10.1038/nature18933

Glasser MF, Goyal MS, Preuss TM, Raichle ME, Van Essen DC. 2014. Trends and properties of human cerebral cortex: Correlations with cortical myelin content. *Neuroimage*. doi:10.1016/j.neuroimage.2013.03.060

Glasser MF, Smith SM, Marcus DS, Andersson JLR, Auerbach EJ, Behrens TEJ, Coalson TS, Harms MP, Jenkinson M, Moeller S, Robinson EC, Sotiropoulos SN, Xu J, Yacoub E, Ugurbil K, Van Essen DC. 2016b. The Human Connectome Project's neuroimaging approach. *Nat Neurosci* **19**:1175–1187. doi:10.1038/nn.4361

Glasser MF, Sotiropoulos SN, Wilson JA, Coalson TS, Fischl B, Andersson JL, Xu J, Jbabdi S, Webster M, Polimeni JR, Van Essen DC, Jenkinson M. 2013. The minimal preprocessing pipelines for the Human Connectome Project. *Neuroimage* **80**:105–124. doi:10.1016/j.neuroimage.2013.04.127

Glasser MF, Van Essen DC. 2011. Mapping Human Cortical Areas In Vivo Based on Myelin Content as Revealed by T1- and T2-Weighted MRI. *J Neurosci* **31**:11597–11616. doi:10.1523/JNEUROSCI.2180-11.2011

Gordon EM, Lynch CJ, Gratton C, Laumann TO, Gilmore AW, Greene DJ, Ortega M, Nguyen AL, Schlaggar BL, Petersen SE, Dosenbach NUF, Nelson SM. 2018. Three Distinct Sets of Connector Hubs Integrate Human Brain Function. *Cell Rep* **24**:1687–1695.e4. doi:10.1016/j.celrep.2018.07.050

Haber SN. 2003. The primate basal ganglia: Parallel and integrative networks. *J Chem Neuroanat* **26**:317–330. doi:10.1016/j.jchemneu.2003.10.003

Halassa MM, Kastner S. 2017. Thalamic functions in distributed cognitive control. *Nat Neurosci* **20**:1669–1679. doi:10.1038/s41593-017-0020-1

Hampson M, Driesen NR, Skudlarski P, Gore JC, Constable RT. 2006. Brain Connectivity Related to Working Memory Performance. *J Neurosci* **26**:13338–13343. doi:10.1523/JNEUROSCI.3408-06.2006

Hugdahl K, Raichle ME, Mitra A, Specht K. 2015. On the existence of a generalized non-specific task-dependent network. *Front Hum Neurosci* **9**:430. doi:10.3389/fnhum.2015.00430

Ji JL, Spronk M, Kulkarni K, Repovš G, Anticevic A, Cole MW. 2019. Mapping the human brain's cortical-subcortical functional network organization. *Neuroimage* **185**:35–57. doi:10.1016/j.neuroimage.2018.10.006

Kemp JM, Powell TP. 1970. The cortico-striate projection in the monkey. *Brain* **93**:525–46. doi:10.1093/brain/93.3.525

King M, Hernandez-Castillo CR, Poldrack RR, Ivry R, Diedrichsen J. 2018. A Multi-Domain Task Battery Reveals Functional Boundaries in the Human Cerebellum. *bioRxiv*. doi:10.1101/423509

Laumann TO, Gordon EM, Adeyemo B, Snyder AZ, Joo SJ, Chen M, Gilmore AW, McDermott KB, Nelson SM, Dosenbach NUF, Schlaggar BL, Mumford JA, Poldrack RA, Petersen SE. 2015. Functional System and Areal Organization of a Highly Sampled Individual Human Brain. *Neuron* **87**:657–670. doi:10.1016/j.neuron.2015.06.037

Luria AR. 1966. Higher cortical functions in man., Higher cortical functions in man. Oxford, England: Basic Books.

Markov NT, Ercsey-Ravasz MM, Ribeiro Gomes AR, Lamy C, Magrou L, Vezoli J, Misery P, Falchier A, Quilodran R, Gariel MA, Sallet J, Gamanut R, Huissoud C, Clavagnier S, Giroud P, Sappey-Marinier D, Barone P, Dehay C, Toroczkai Z, Knoblauch K, Van Essen DC, Kennedy H. 2014. A weighted and directed interareal

connectivity matrix for macaque cerebral cortex. *Cereb Cortex* **24**:17–36. doi:10.1093/cercor/bhs270

Michalka SW, Kong L, Rosen ML, Shinn-Cunningham BG, Somers DC. 2015. Short-Term Memory for Space and Time Flexibly Recruit Complementary Sensory-Biased Frontal Lobe Attention Networks. *Neuron* **87**:882–892. doi:10.1016/j.neuron.2015.07.028

Middleton FA, Strick PL. 2000. Basal ganglia and cerebellar loops: Motor and cognitive circuits. *Brain Res Rev* **31**:236–250. doi:10.1016/S0165-0173(99)00040-5

Miller EK, Cohen JD. 2001. An integrative theory of prefrontal cortex function. *Annu Rev Neurosci* **24**:167–202.

Miller GA, Galanter E, Pribram KH. 1968. Plans and the Structure of Behavior. *J Oper Res Soc*. doi:10.1057/jors.1968.86

Milner B. 1963. Effects of different brain lesions on card sorting: The role of the frontal lobes. *Arch Neurol* **9**:90–100. doi:10.1001/archneur.1963.00460070100010

Mitchell DJ, Bell AH, Buckley MJ, Mitchell AS, Sallet J, Duncan J. 2016. A Putative Multiple-Demand System in the Macaque Brain. *J Neurosci* **36**:8574–8585. doi:10.1523/JNEUROSCI.0810-16.2016

Naya Y, Chen H, Yang C, Suzuki WA. 2017. Contributions of primate prefrontal cortex and medial temporal lobe to temporal-order memory. *Proc Natl Acad Sci* **114**:13555–13560. doi:10.1073/pnas.1712711114

Newell A. 1990. Unified Theories of Cognition. Cambridge, MA, USA: Harvard University Press.

Norman DA, Shallice T. 1986. Attention to action: Willed and automatic control of behaviour (Revised reprint of Norman and Shallice (1980))Consciousness and Self-Regulation: Advances in Research and Theory. pp. 1–18.

Öngür D, Ferry AT, Price JL. 2003. Architectonic subdivision of the human orbital and medial prefrontal cortex. *J Comp Neurol* **460**:425–449. doi:10.1002/cne.10609

Parthasarathy A, Herikstad R, Bong JH, Medina FS, Libedinsky C, Yen SC. 2017. Mixed selectivity morphs population codes in prefrontal cortex. *Nat Neurosci* **20**:1770–1779. doi:10.1038/s41593-017-0003-2

Petersen SE, Sporns O. 2015. Brain Networks and Cognitive Architectures. *Neuron* **88**:207–219. doi:10.1016/j.neuron.2015.09.027

Petrides M, Pandya DN. 1999. Dorsolateral prefrontal cortex: comparative cytoarchitectonic analysis in the human and the macaque brain and corticocortical connection patterns. *Eur J Neurosci* **11**:1011–1036. doi:10.1046/j.1460-9568.1999.00518.x

Pobric G, Jefferies E, Ralph MAL. 2007. Anterior temporal lobes mediate semantic representation: Mimicking semantic dementia by using rTMS in normal participants.

Proc Natl Acad Sci **104**:20137–20141. doi:10.1073/pnas.0707383104

Power JD, Cohen AL, Nelson SM, Wig GS, Barnes KA, Church JA, Vogel AC, Laumann TO, Miezin FM, Schlaggar BL, Petersen SE. 2011. Functional Network Organization of the Human Brain. *Neuron* **72**:665–678. doi:10.1016/j.neuron.2011.09.006

Power JD, Schlaggar BL, Lessov-Schlaggar CN, Petersen SE. 2013. Evidence for hubs in human functional brain networks. *Neuron* **79**:798–813. doi:10.1016/j.neuron.2013.07.035

Premereur E, Janssen P, Vanduffel W. 2018. Functional MRI in Macaque Monkeys during Task Switching. *J Neurosci* **38**:10619–10630. doi:10.1523/JNEUROSCI.1539-18.2018

Ramnani N. 2006. The primate cortico-cerebellar system: anatomy and function. *Nat Rev Neurosci* **7**:511–522. doi:10.1038/nrn1953

Ramnani N, Owen AM. 2004. Anterior prefrontal cortex: insights into function from anatomy and neuroimaging. *Nat Rev Neurosci* **5**:184–194. doi:10.1038/nrn1343

Rigotti M, Barak O, Warden MR, Wang XJ, Daw ND, Miller EK, Fusi S. 2013. The importance of mixed selectivity in complex cognitive tasks. *Nature* **497**:585–590. doi:10.1038/nature12160

Robinson EC, Garcia K, Glasser MF, Chen Z, Coalson TS, Makropoulos A, Bozek J, Wright R, Schuh A, Webster M, Hutter J, Price A, Cordero Grande L, Hughes E, Tusor N, Bayly P V., Van Essen DC, Smith SM, Edwards AD, Hajnal J, Jenkinson M, Glocker B, Rueckert D. 2018. Multimodal surface matching with higher-order smoothness constraints. *Neuroimage* **167**:453–465. doi:10.1016/j.neuroimage.2017.10.037

Robinson EC, Jbabdi S, Glasser MF, Andersson J, Burgess GC, Harms MP, Smith SM, Van Essen DC, Jenkinson M. 2014. MSM: A new flexible framework for multimodal surface matching. *Neuroimage* **100**:414–426. doi:10.1016/j.neuroimage.2014.05.069

Roca M, Parr A, Thompson R, Woolgar A, Torralva T, Antoun N, Manes F, Duncan J. 2010. Executive function and fluid intelligence after frontal lobe lesions. *Brain* **133**:234–247. doi:10.1093/brain/awp269

Salimi-Khorshidi G, Douaud G, Beckmann CF, Glasser MF, Griffanti L, Smith SM. 2014. Automatic denoising of functional MRI data: Combining independent component analysis and hierarchical fusion of classifiers. *Neuroimage* **90**:449–468. doi:10.1016/j.neuroimage.2013.11.046

Sigala N, Kusunoki M, Nimmo-Smith I, Gaffan D, Duncan J. 2008. Hierarchical coding for sequential task events in the monkey prefrontal cortex. *Proc Natl Acad Sci U S A* **105**:11969–11974. doi:10.1073/pnas.0802569105

Smith SM, Vidaurre D, Beckmann CF, Glasser MF, Jenkinson M, Miller KL, Nichols TE, Robinson EC, Salimi-Khorshidi G, Woolrich MW, Barch DM, Uğurbil K, Van Essen

DC. 2013. Functional connectomics from resting-state fMRI. *Trends Cogn Sci* **17**:666–682. doi:10.1016/j.tics.2013.09.016

Sporns O. 2014. Contributions and challenges for network models in cognitive neuroscience. *Nat Neurosci* **17**:652–660. doi:10.1038/nn.3690

Stokes MG, Kusunoki M, Sigala N, Nili H, Gaffan D, Duncan J. 2013. Dynamic coding for cognitive control in prefrontal cortex. *Neuron* **78**:364–375. doi:10.1016/j.neuron.2013.01.039

Uğurbil K, Xu J, Auerbach EJ, Moeller S, Vu AT, Duarte-Carvajalino JM, Lenglet C, Wu X, Schmitter S, Van de Moortele PF, Strupp J, Sapiro G, De Martino F, Wang D, Harel N, Garwood M, Chen L, Feinberg DA, Smith SM, Miller KL, Sotiropoulos SN, Jbabdi S, Andersson JLR, Behrens TEJ, Glasser MF, Van Essen DC, Yacoub E. 2013. Pushing spatial and temporal resolution for functional and diffusion MRI in the Human Connectome Project. *Neuroimage* **80**:80–104. doi:10.1016/j.neuroimage.2013.05.012

Van Essen DC, Glasser MF. 2018. Parcellating Cerebral Cortex: How Invasive Animal Studies Inform Noninvasive Mapmaking in Humans. *Neuron* **99**:640–663. doi:10.1016/j.neuron.2018.07.002

Van Essen DC, Glasser MF, Dierker DL, Harwell J, Coalson T. 2012. Parcellations and hemispheric asymmetries of human cerebral cortex analyzed on surface-based atlases. *Cereb Cortex* **22**:2241–2262. doi:10.1093/cercor/bhr291

Visser M, Jefferies E, Lambon Ralph MA. 2010. Semantic Processing in the Anterior Temporal Lobes: A Meta-analysis of the Functional Neuroimaging Literature. *J Cogn Neurosci* **22**:1083–1094. doi:10.1162/jocn.2009.21309

Warren DE, Power JD, Bruss J, Denburg NL, Waldron EJ, Sun H, Petersen SE, Tranel D. 2014. Network measures predict neuropsychological outcome after brain injury. *Proc Natl Acad Sci* **111**:14247–14252. doi:10.1073/pnas.1322173111

Woolgar A, Duncan J, Manes F, Fedorenko E. 2018. Fluid intelligence is supported by the multiple-demand system not the language system. *Nat Hum Behav* **2**:200–204. doi:10.1038/s41562-017-0282-3

Woolgar A, Hampshire A, Thompson R, Duncan J. 2011. Adaptive Coding of Task-Relevant Information in Human Frontoparietal Cortex. *J Neurosci* **31**:14592–14599. doi:10.1523/JNEUROSCI.2616-11.2011

Woolgar A, Jackson J, Duncan J. 2016. Coding of Visual, Auditory, Rule, and Response Information in the Brain: 10 Years of Multivoxel Pattern Analysis. *J Cogn Neurosci* **28**:1433–1454. doi:10.1162/jocn

Woolgar A, Parr A, Cusack R, Thompson R, Nimmo-Smith I, Torralva T, Roca M, Antoun N, Manes F, Duncan J. 2010. Fluid intelligence loss linked to restricted regions of damage within frontal and parietal cortex. *Proc Natl Acad Sci U S A* **107**:14899–14902. doi:10.1073/pnas.1007928107

Yeo BTT, Krienen FM, Sepulcre J, Sabuncu MR, Lashkari D, Hollinshead M, Roffman

JL, Smoller JW, Zöllei L, Polimeni JR, Fischl B, Liu H, Buckner RL. 2011. The organization of the human cerebral cortex estimated by intrinsic functional connectivity. *J Neurophysiol* **106**:1125–1165. doi:10.1152/jn.00338.2011

Yeterian EH, Pandya DN. 1991. Prefrontostriatal connections in relation to cortical architectonic organization in rhesus monkeys. *J Comp Neurol* **312**:43–67. doi:10.1002/cne.903120105